JOURNAL OF COMPUTATIONAL PHYSICS 101, 386–418 (1992)

Absorbing Boundary Conditions for Acoustic and Elastic Waves in Stratified Media

ROBERT L. HIGDON

Department of Mathematics, Oregon State University, Corvallis, Oregon 97331

Received October 16, 1990; revised August 9, 1991

Absorbing boundary conditions are needed for computing numerical models of wave motions in unbounded spatial domains. Prior progress on this problem for acoustic and elastic waves has generally been concerned with waves propagating through uniform media. The present paper is concerned with waves in stratified media, which are of interest, for example, in geophysical problems. Suppose that the medium consists of homogeneous layers separated by parallel horizontal interfaces, and suppose that absorbing boundary conditions are needed along a vertical computational boundary. The boundary conditions that are described in this paper are based on a quantity known as the "ray parameter." According to Snell's law, this parameter remains the same when a plane wave propagates through a stratified medium and undergoes reflection, refraction, and, in the case of elastic waves, conversion. Once can therefore use the same absorbing boundary conditions in all layers. For acoustic waves, the absorption properties are the same in all layers. For elastic waves, the absorption properties vary somewhat from one layer to another; however, one still obtains good absorption in all layers, even in the presence of strong contrasts between layers. The boundary conditions are also effective in absorbing Rayleigh waves, which propagate along free surfaces of elastic media. The boundary formulas developed here can be applied without modification to problems in both two and three dimensions.

1. INTRODUCTION

Absorbing boundary conditions for acoustic and elastic waves have been the subject of a great deal of research in recent years. Most, if not all, of the progress on this subject has been concerned with wave propagation in homogeneous media. However, nonhomogeneous media are encountered in many applications. In this paper, we consider the particular case of layered media, which are of interest, for example, in geophysical problems. We show that the absorbing boundary conditions developed by the author in [8–10] for homogeneous media are also effective in the present situation, even in the case of strong contrasts between layers. For the case of elastic waves, the boundary conditions are also shown to be effective near a free surface.

The motivation for this work is as follows. In many physical problems, the spatial domain is unbounded. However, when a numerical solution to such a problem is computed, it is necessary to reduce the problem to a bounded domain of manageable size. A typical approach is simply to truncate the original physical domain. It then becomes necessary to find boundary conditions to impose at the artificial computational boundary that is thereby introduced. If the physical process is a wave motion that arises entirely within the computational domain and if there are no mechanisms beyond the computational boundary that cause reflection back toward that domain, then the solution near the boundary consists of outgoing wave motions. It is then reasonable to seek boundary conditions that simulate the outward radiation of energy. The classical Dirichlet boundary condition is unsuitable for this purpose, as it generates large reflections back into the interior, and these reflections degrade the solution that is computed. Instead, one wants "absorbing" boundary conditions which generate little or no reflection.

In the configuration examined in this paper, the spatial domain consists of homogeneous layers separated by parallel horizontal interfaces, and the principal problem is to study absorbing boundary conditions that are imposed along a vertical computational boundary. (Along a horizontal computational boundary, the medium is locally homogeneous, so in that case the behavior of absorbing boundary conditions is the same as for homogeneous media.) It is assumed that a wave is moving downward through the uppermost layer, and this wave then generates wave motions in lower layers. In some numerical computations involving elastic waves that are described later, the medium also includes a horizontal free surface at the top of the uppermost layer, and waves also propagate along this surface.

Prior work on absorbing boundary conditions for acoustic or elastic waves includes [3, 5–12, 14, 16, 18–21]. For various reasons, this work has generally been restricted to media that are homogeneous near the computational boundary. In some cases, the restriction arises from the use of Fourier transforms in the direction parallel to the bound-

0021-9991/92 $5.00

ary, which is valid if the medium is uniform in that direction. These transforms have been used in the derivation and/or analysis of boundary conditions (e.g., [3, 5, 6, 8–10, 14, 16, 21]) and have also been used explicitly in computational algorithms (e.g., [18]). A related issue is that absorbing boundary conditions frequently involve derivatives in the direction parallel to the boundary. If such a boundary condition is approximated by finite differences, the discrete boundary operator will then involve tangential shifts; the tangential derivatives are typically of even order, and the corresponding difference approximations are generally centered. On the other hand, one might want one-sided differencing or no tangential differencing at all at points where a computational boundary intersects an interface, due to discontinuities in the material parameters. Analogous remarks apply to a point where a computational boundary intersects a free surface and to other corners of the computational domain.

In physical terms, some difficulties with stratified media can be described as follows: Suppose that a plane acoustic or elastic wave is incident upon a discontinuity in the medium. In general, the wave does not simply pass without modification through the interface, but instead can be reflected and/or refracted at the interface. In the case of elastic waves, there is an additional complication. In the interior of an elastic medium, there can be two kinds of waves: P-waves (primary, or compressional) and S-waves (secondary, or shear). For P-waves, the particle motions are parallel to the direction of wave propagation; for S-waves, the particle motions are perpendicular to the direction of propagation. During the process of reflection and/or refraction, each type of wave can be partially or totally converted to the other type. Overall, for either acoustic or elastic waves, a single incident wave can produce a wave system of great complexity if several interfaces are present. In principle, this situation can lead to problems in constructing and analyzing boundary conditions that are capable of giving good absorption for all of the various waves in this system.

A unifying principle for wave propagation in stratified media is given by Snell's law, which states that a certain parameter (the "ray parameter") remains invariant under reflection and refraction, and, in the case of elastic body waves, also under conversion. A main point of the present paper is that the absorbing boundary conditions developed by the author in [8–10] can be interpreted as being based on this parameter. This implies that along a vertical computational boundary in a horizontally stratified medium, one can apply the same boundary operator in all layers. The operators that are used for acoustic waves are very similar to the ones that are used for elastic waves. For acoustic waves, it will be shown that the absorption properties of the boundary conditions are independent of the layer. For elastic waves, which are more complicated, this is not quite the case. However, the absorption properties do not vary greatly from one layer to another, and the boundary conditions yield good absorption in all layers, even in the presence of strong contrasts between layers.

The boundary conditions can be approximated by finite difference equations that use values of the solution only along grid lines that are perpendicular to the boundary. These difference equations have the following advantages. First, the same formulas apply without modification to problems in both two and three dimensions. Second, for reasons discussed in Section 4, the one-dimensional stencil provides for convenient implementation near interfaces, near a free surface, and near corners. Third, at each time step, each horizontal grid row is independent of other horizontal rows, provided that an explicit difference scheme is used in the interior. This is useful if solutions are computed in parallel.

Some empirical investigations [4, 17] have suggested that various earlier absorbing boundary conditions for elastic waves may be unstable if the ratio of S-wave velocity to P-wave velocity is sufficiently low. Low values of this ratio are found in materials of relatively low rigidity, including some that are of interest in seismic petroleum exploration. However, a low value of the velocity ratio does not cause instability with the boundary conditions that are developed in the present paper. For further discussion, see Test 2 in Section 5.

An outline of the remainder of the paper is as follows. Absorbing boundary conditions for acoustic waves and for elastic waves are analyzed in Sections 2 and 3, respectively. Difference approximations to these boundary conditions are developed in Section 4. This section also describes how the difference approximations can be coordinated with free-surface and interface conditions for elastic waves. The results of some numerical computations are given in Section 5.

2. ACOUSTIC WAVES

Absorbing boundary conditions for acoustic waves were developed by the author in [8, 9]. The goal of the present section is to show that when these boundary conditions are applied along a vertical computational boundary, the absorption properties depend only on the ratio of horizontal wavenumber to time frequency. In a horizontally stratified medium, these quantities do not vary from one layer to another. Effective absorption can therefore be obtained by using the same boundary operator in each layer.

2.1. Formulas for Boundary Conditions in Homogeneous and Layered Media

We first summarize some properties of the boundary conditions for the case of a homogeneous medium. Consider the

acoustic wave equation $u_{tt} = c^2 \nabla^2 u$ in either two or three space dimensions. Let x denote the horizontal coordinate perpendicular to the computational boundary; suppose that the computational domain corresponds to $x > 0$; and let z be the vertical coordinate, with positive direction downward. In this notation, the boundary conditions at $x = 0$ have the form

$$\left[\prod_{j=1}^{m} \left((\cos \alpha_j)\frac{\partial}{\partial t} - c\frac{\partial}{\partial x}\right)\right] u = 0, \tag{2.1}$$

where $|\alpha_j| < \pi/2$ for all j. Boundary conditions of this type were also derived independently by Keys [14]. In practice, one would use $m = 2$ or possibly $m = 3$. Difference approximations to (2.1) are discussed in Section 4.

The form (2.1) provides a general representation of absorbing boundary conditions for the acoustic wave equation, in a sense described in Proposition 9.1 of [8]. For example, the boundary conditions of Engquist and Majda [5, 6] are equivalent to (2.1) with $\alpha_j = 0$ for all j, and the boundary conditions of Trefethen and Halpern [21] are equivalent to (2.1) for various nonzero α_j's.

A motivation for the form of (2.1) is the following. For definiteness, consider the case of two dimensions; a similar discussion applies to three-dimensional problems. The purpose of the boundary conditions is to simulate the outward radiation of energy from the interior of the computational domain. To do this, we seek boundary conditions that are satisfied by outgoing waves, at least in an approximate sense. An example of an outgoing wave is given by a plane wave of the form

$$\begin{aligned} u(x, z, t) &= f((x, z - z_0) \cdot (\cos \alpha, \sin \alpha) + ct) \\ &= f(x \cos \alpha + (z - z_0) \sin \alpha + ct), \end{aligned} \tag{2.2}$$

where z_0 is any reference point along the z-axis, and f is an arbitrary function. The wave (2.2) travels out of the domain $x > 0$ with speed c at angle of incidence α relative to normal incidence. When the operator

$$(\cos \alpha)\frac{\partial}{\partial t} - c\frac{\partial}{\partial x} \tag{2.3}$$

is applied to (2.2), the result is zero. The boundary condition (2.1) is therefore satisfied exactly by any linear combination of outgoing plane waves traveling with speed c at angles of incidence $\pm\alpha_1, \ldots, \pm\alpha_m$. It is then possible to show that no reflected waves will be present in this case, since the boundary condition is entirely compatible with the outward radiation of energy.

More generally, suppose that a sinusoidal plane wave approaches the boundary at an arbitrary angle of incidence θ. In general, this wave will not satisfy the boundary condition (2.1) exactly. The solution that is obtained must then include a reflected wave, so that the superposition of incident and reflected waves does satisfy the boundary condition. The ratio of the amplitudes of the reflected and incident waves is given by the reflection coefficient

$$R(\theta) = \prod_{j=1}^{m} \left|\frac{\cos \alpha_j - \cos \theta}{\cos \alpha_j + \cos \theta}\right| \tag{2.4}$$

(see Section 2.2). Each factor in (2.4) is less than 1 if $|\theta| < \pi/2$, and the zeros of R are the angles of perfect absorption. Numerical experiments have shown that good performance can be obtained by using second-order ($m = 2$) or possibly third-order ($m = 3$) versions of (2.1).

The zeros $\pm\alpha_1, \ldots, \pm\alpha_m$ of the reflection coefficient appear as explicit parameters in the boundary condition (2.1), and this creates the possibility of easily adapting the boundary condition to a priori information about the solution, if available. Numerical experiments have shown that the performance of the boundary condition is not very sensitive to the choice of α_j's; Test 1 in Section 5 gives an example for the analogous case of elastic waves. In practice, it would suffice to make some rough estimates for these parameters and not worry about experimentation or fine-tuning. An optimal choice of parameters would be problem-dependent.

Now suppose that absorbing boundary conditions are imposed along a vertical computational boundary in a horizontally layered medium having different wave velocities in the various layers. The differing velocities would appear to complicate the process of choosing the parameters in the boundary condition (2.1). However, it will be shown here that the same boundary operator can be applied in all layers.

For the sake of simplicity, the following discussion is concerned with a medium consisting of two layers, and the wave velocities in the upper and lower layers will be denoted by c and c', respectively. The conclusions that are obtained can be applied to media having more than two layers.

Suppose that the plane wave (2.2) moves downward through the upper layer. In general, a portion of the wave's energy can be reflected upward from the interface, and a portion can be transmitted through the interface. Suppose that the transmitted wave is a propagating plane wave, and let α' denote the angle of incidence relative to the vertical computational boundary (see Fig. 2.1). The direction of propagation in the lower layer is determined by Snell's law of refraction, which states that the waves in the two layers must have the same "apparent velocity." This quantity is the velocity of a point where a wavefront intersects a horizontal line (for example, the point P in Fig. 2.1); equivalently, it is the velocity seen by an observer who restricts attention to a horizontal line. The apparent velocities in the two layers are

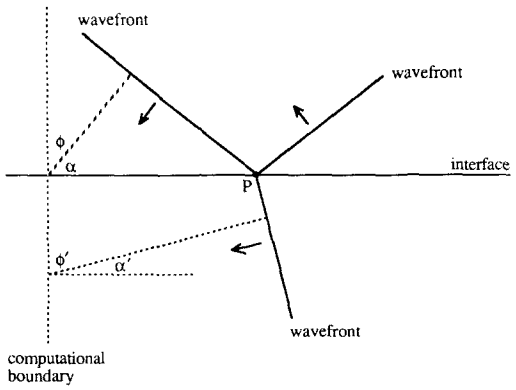

FIG. 2.1. Illustration of angles of incidence. The arrows represent directions of propagation.

$c/\cos\alpha$ and $c'/\cos\alpha'$, so $c/\cos\alpha = c'/\cos\alpha'$. Equivalently, if ϕ and ϕ' denote angles of incidence relative to the horizontal interface (instead of the vertical computational boundary), then $c/\sin\phi = c'/\sin\phi'$. The reciprocal of the apparent velocity is known as the "ray parameter" (see, e.g., Aki and Richards [1]).

The operator (2.3) is a constant multiple of

$$\frac{\partial}{\partial t} - \left(\frac{c}{\cos\alpha}\right)\frac{\partial}{\partial x}, \tag{2.5}$$

so the operator (2.3) can be regarded as based on the ray parameter. This operator yields exact absorption of the wave (2.2), and it also gives exact absorption of the wave that is obtained when (2.2) is reflected from the interface, since the reflected wave approaches the computational boundary at angle of incidence $-\alpha$. In order to absorb the transmitted wave in the lower layer, one could use the operator $\partial/\partial t - (c'/\cos\alpha')\,\partial/\partial x$. By Snell's law, this is identical to (2.5), so one can use the same operator in both layers.

If $c' > c$, then Snell's law yields $\cos\alpha' > 1$ when $\cos\alpha$ is sufficiently close to 1. As will be discussed later, the transmitted wave in this case is not a propagating plane wave, but instead is an "evanescent" wave that decays with depth and propagates horizontally. In this case, it is not really appropriate to speak in terms of angles of incidence. For this reason, we adopt a more general notation for the absorbing boundary conditions in the two layers.

In the upper layer, we consider boundary conditions of the form

$$B(\partial/\partial x, \partial/\partial t)u = \left[\prod_{j=1}^{m}\left(\beta_j\frac{\partial}{\partial t} - c\frac{\partial}{\partial x}\right)\right]u = 0, \tag{2.6a}$$

where each β_j is a positive dimensionless constant. If $\beta_j \leqslant 1$, then β_j can be regarded as the cosine of an angle of perfect absorption for waves having speed c. The boundary condition (2.6a) will also be applied in the lower layer; equivalently, one can think in terms of applying the boundary condition

$$B'(\partial/\partial x, \partial/\partial t)u = \left[\prod_{j=1}^{m}\left(\beta_j'\frac{\partial}{\partial t} - c'\frac{\partial}{\partial x}\right)\right]u = 0 \tag{2.6b}$$

in the lower layer, where $\beta_j/\beta_j' = c/c'$. This would avoid the notational annoyance of using a wave speed c in the boundary condition for the lower layer which is different from the wave speed c' that is actually present in that layer. However, this distinction is not an issue when (2.6a) and (2.6b) are implemented using finite differences. In Section 4 it is shown that the boundary condition (2.6a) can be approximated by a finite-difference equation that is determined by the dimensionless parameters $\beta_1, \ldots, \beta_m$ and the Courant number $\nu = c\,\Delta t/\Delta x$, which is also dimensionless. In practice, one specifies the same values of these parameters in each layer. Further comments on this matter are given after Eq. (4.5).

As a practical procedure, one could select the β_j's by considering angles of incidence in the upper layer. For reasons given earlier, the lower layer would then be handled properly automatically. An exception to this procedure can arise if the lower layer is faster than the upper layer and if a "head wave" is generated when a cylindrical or spherical wave moves downward into the lower layer. An analogous situation for elastic waves is shown in Test 3 in Section 5. As illustrated in that section, it is advisable to tune one of the factors in the boundary operator to give exact absorption of a normally incident wave in the lower (faster) layer. In the context of (2.6), this would mean $\beta_j' = 1$, or $\beta_j = c/c' < 1$.

2.2. Calculation of Reflection Coefficients

We now calculate reflection coefficients at the computational boundary for (2.6a) and (2.6b) in the two layers. For the sake of definiteness, we work with two-dimensional problems; the same analysis also applies to problems in three dimensions, except for the obvious differences in notation.

The calculation is based on oscillatory plane waves of the form $u(x, z, t) = \exp(ikx + ilz - i\omega t)$. A wave of this type is a solution of $u_{tt} = c^2(u_{xx} + u_{zz})$ if and only if the dispersion relation $\omega^2 = c^2(k^2 + l^2)$ is satisfied. The graph of this relation is a double cone in (k, l, ω) space. For waves of the present form, the group and phase velocities coincide and are equal to $c(ck/\omega, cl/\omega)$. Therefore, for waves moving into (out of) the domain $x > 0$, k and ω must have the same (opposite) signs. The unit vector $(ck/\omega, cl/\omega)$ represents the direction of propagation. If θ is the angle of incidence relative to the inward normal to the computational boundary, then $\cos\theta = ck/\omega$ for incoming waves and $\cos\theta = -ck/\omega$ for outgoing waves.

In order to determine reflection properties of (2.6a) in the upper layer, consider a linear combination

$$a_1 e^{ik_1 x + ilz - i\omega t} + a_2 e^{ik_2 x + ilz - i\omega t}. \tag{2.7}$$

Here, k_1 and k_2 are chosen to correspond to incoming and outgoing waves, respectively, so $k_2 = -k_1$. The same dependences with respect to z and t are chosen in order that the linear combination can satisfy a boundary condition identically at $x = 0$. The coefficient a_2 of the outgoing wave is assumed to be known, and the problem is to determine the coefficient a_1 of the incoming wave. We want the ratio $|a_1/a_2|$ to be as small as possible.

When (2.7) is inserted into the boundary condition (2.6a), the result is

$$a_1 B(ik_1, -i\omega) + a_2 B(ik_2, -i\omega) = 0.$$

The amplitude reflection coefficient is $R = |a_1/a_2|$, so

$$\begin{aligned} R &= \left| \frac{B(ik_2, -i\omega)}{B(ik_1, -i\omega)} \right| \\ &= \prod_{j=1}^{m} \left| \frac{\beta_j(-i\omega) - c(ik_2)}{\beta_j(-i\omega) - c(ik_1)} \right| \\ &= \prod_{j=1}^{m} \left| \frac{-\beta_j - ck_2/\omega}{-\beta_j - ck_1/\omega} \right|. \end{aligned} \tag{2.8}$$

A traditional way of representing reflection coefficients is to write them as functions of angle of incidence (e.g., [3, 5, 14, 16, 18]). In the present case, this can be done by observing $ck_1/\omega = \cos\theta$ and $ck_2/\omega = -\cos\theta$. The result is equivalent to (2.4) if $\beta_j = \cos\alpha_j$ for all j.

However, in discussions of layered media, it is not very desirable to represent reflection coefficients in this manner. If the transmitted wave is a propagating wave, then its angle of incidence is different from that of the wave in the upper layer. For the sake of clarity, it would be useful to express reflection coefficients in terms of a quantity that is the same in both layers. Also, for reasons given later, if $c' < c$ then there are angles of incidence in the lower layer that cannot actually be seen if the wave in the lower layer is generated by a wave moving downward through the upper layer. In this case, a formula for reflection coefficients in terms of angle of incidence would contain irrelevant information. On the other hand, if $c' > c$, then there are transmitted waves that are evanescent and thus do not have a real angle of incidence, and a formula involving angles of incidence would be incomplete. We therefore develop an alternate method for representing reflection coefficients in the two layers.

We begin with a summary of the wave forms that can be found in the lower layer. If a wave $\exp(ikx + ilz - i\omega t)$ moves downward through the upper layer, then the wave that is generated in the lower layer must be a constant multiple of a wave having the form $\exp(ikx + \gamma z - i\omega t)$. The same dependences with respect to x and t are used in order that physical boundary conditions can be satisfied identically along the interface, which corresponds to a constant value of z (see, e.g., Aki and Richards [1]). The wave equation in the lower layer implies $(-i\omega)^2 = (c')^2((ik)^2 + \gamma^2)$, so γ can be either real or purely imaginary. If γ is real, we assume $\gamma < 0$ in order to prevent the wave amplitude from being unbounded as $z \to +\infty$. (We have assumed that the positive z-direction is downward.) In this case, the wave propagates in x and decays with respect to z, and the wave is evanescent.

Our goal is to represent the reflection coefficients in the two layers in terms of k and ω, which are the same in both layers. We also develop a geometrical interpretation of reflection coefficients which helps to clarify the issue of which waves can actually be seen in the lower layer.

The reflection coefficient (2.8) for the upper layer can be written as

$$R = \prod_{j=1}^{m} \left| \frac{-\beta_j + s}{-\beta_j - s} \right|, \tag{2.9}$$

where $s = ck_1/\omega = |ck_2/\omega|$. For a wave of the form $\exp(ikx + ilz - i\omega t)$, the quantity ck/ω will be referred to as a scaled horizontal wavenumber, since the horizontal wavenumber k is scaled to be dimensionless. Similarly, the quantity cl/ω can be regarded as a scaled vertical wavenumber. The dispersion relation $\omega^2 = c^2(k^2 + l^2)$ for the wave equation implies $(ck/\omega)^2 + (cl/\omega)^2 = 1$, so the set of all possible scaled wavenumbers for the upper layer is the unit circle shown in Fig. 2.2. In this diagram, a vector from the origin to $(ck/\omega, cl/\omega)$ gives the direction of propagation in (x, z) space. Waves moving at normal incidence to the computational boundary correspond to $s = 1$, and waves moving parallel to the boundary correspond to $s = 0$.

The jth factor in the reflection coefficient (2.9) can be interpreted in terms of this diagram. Regard $-\beta_j$ as a coordinate along the negative "ck/ω" axis. The numerator in this factor is the distance from the line $ck/\omega = -\beta_j$ to the point on the circle having horizontal coordinate ck_2/ω; this point corresponds to an outgoing wave. The denominator is the distance from $-\beta_j$ to the point having horizontal coordinate ck_1/ω, which corresponds to an incoming wave. The ratio of the distances is less than 1, except when $ck_1/\omega = ck_2/\omega = 0$, which is the case of waves traveling parallel to the boundary $x = 0$. The ratio is zero at points where the line $ck/\omega = -\beta_j$ intersects the circle, so the jth factor in the boundary operator in (2.6a) yields perfect absorption in that case.

We now consider the lower layer. In order to facilitate comparisons with the upper layer, the wavenumbers will be

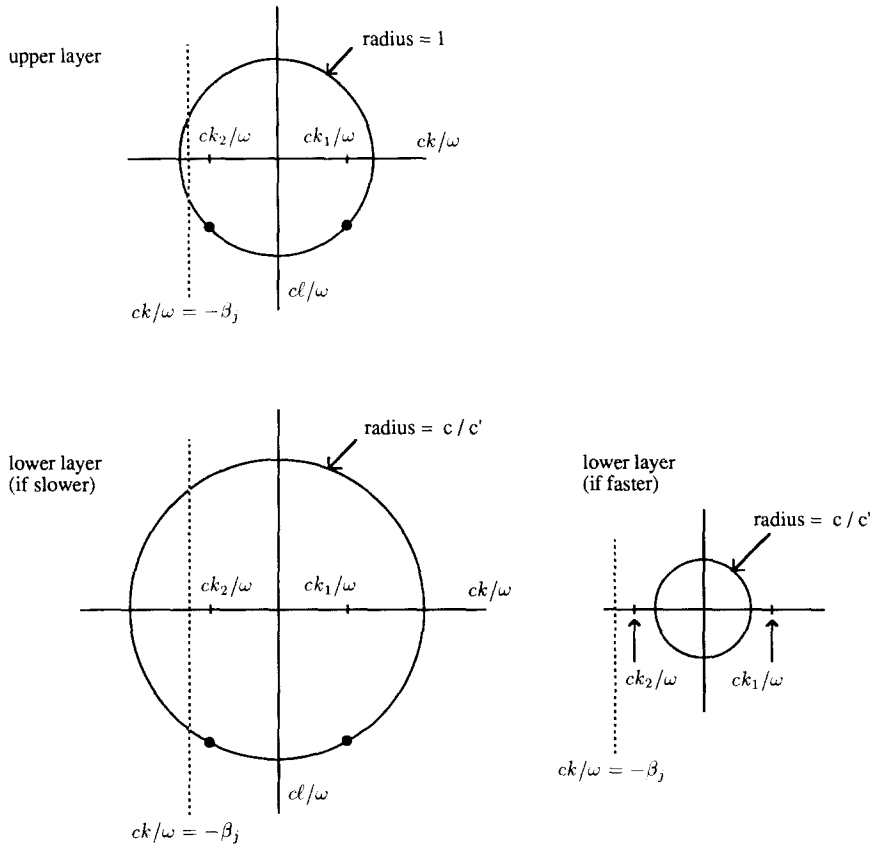

FIG. 2.2. Diagrams of the scaled wavenumbers that are involved in the reflection analysis for acoustic waves. The dimensionless quantity ck/ω is a scaled horizontal wavenumber, and cl/ω is a scaled vertical wavenumber. The graph in the lower left (right) describes the situation in the lower layer if the wave velocity is smaller (larger) than in the upper layer. The velocities in the upper and lower layers are denoted by c and c', respectively. Incoming and outgoing waves correspond to $ck/\omega > 0$ and $ck/\omega < 0$, respectively. Points on the line $ck/\omega = -\beta_j$ correspond to waves that are absorbed exactly by the jth factor in the boundary operator.

scaled in the same manner as before. For purely oscillatory waves $\exp(ikx + il'z - i\omega t)$ in the lower layer, the wave equation implies $\omega^2 = (c')^2\,(k^2 + (l')^2)$, so $(ck/\omega)^2 + (cl'/\omega)^2 = (c/c')^2$. The set of all scaled horizontal and vertical wavenumbers for oscillatory waves must therefore lie on a circle of radius c/c'. If $c' < c$ (i.e., the lower layer is slower than the upper layer), then this circle has radius greater than 1; if $c' > c$, the circle has radius less than 1. Each of these cases is illustrated in Fig. 2.2.

The waves in the two layers must have the same scaled horizontal wavenumber, since k and ω are the same in both layers. If $c' < c$, the wave in the lower layer must always be purely oscillatory, since the circle in Fig. 2.2 for this case is larger than the circle for the upper layer. A comparison of directions of propagation for fixed ck/ω shows that the direction of propagation in the lower layer is closer to vertical, so the wavefronts are closer to horizontal. The larger circle for the lower layer also implies that there are wave motions $\exp(ikx + il'z - i\omega t)$ that satisfy the wave equation in the lower layer but cannot be generated by an oscillatory wave moving downward through the upper layer; this case corresponds to $|ck/\omega| > 1$. For example, if $c' = c/2$, then the circle for the lower layer has radius 2, and the nonobservable waves have angles of incidence 0° through 60°.

Next suppose $c' > c$, i.e., the lower layer is faster than the upper layer. In this case, the circle in Fig. 2.2 for the lower layer is smaller than the circle for the upper layer, so all angles of incidence are possible in the lower layer. Furthermore, if $1 \geqslant |ck/\omega| \geqslant c/c'$, then an oscillatory wave $\exp(ikx + ilz - i\omega t)$ in the upper layer cannot generate an oscillatory wave in the lower layer, since the scaled horizontal wavenumber ck/ω does not correspond to any point on the circle for the lower layer. Instead, the transmitted wave must be evanescent.

In order to calculate a reflection coefficient in the lower layer, consider a linear combination

$$a_1 e^{ik_1 x + \gamma z - i\omega t} + a_2 e^{ik_2 x + \gamma z - i\omega t}. \tag{2.10}$$

As before, k_1 and k_2 are chosen to correspond to incoming and outgoing waves, respectively, and $k_2 = -k_1$. If $c' < c$, then γ is purely imaginary; if $c' > c$, then γ is either

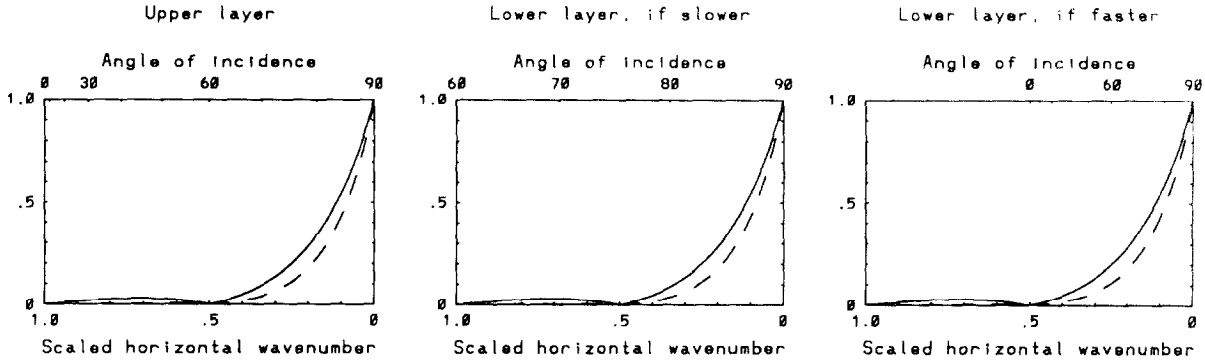

FIG. 2.3. Reflection coefficients for acoustic waves, when written as functions of $s = |ck/\omega|$. Here, k is the horizontal wavenumber of the outgoing wave, and ω is the frequency. The quantity s is invariant under reflection and refraction at the interface. Solid curves show reflection coefficients for the second-order ($m = 2$) absorbing boundary condition, with $\beta_1 = 1$ and $\beta_2 = \cos 60°$. Dashed curves correspond to the third-order ($m = 3$) boundary condition, with $\beta_1 = 1$, $\beta_2 = \cos 60°$, and $\beta_3 = \cos 30°$. Left frame: upper layer. Middle frame: lower layer, when the wave velocity is one-half that of the upper layer. Right frame: lower layer, when the wave velocity is twice as large as in the upper layer. In a sense, the reflection coefficients are plotted as functions of the wave, and the coefficients are the same in both layers.

imaginary or real and negative. When (2.10) is inserted into the boundary condition (2.6b) for the lower layer, the result is

$$R = |a_1/a_2| = \prod_{j=1}^{m} \left| \frac{-\beta_j' - c'k_2/\omega}{-\beta_j' - c'k_1/\omega} \right|$$

$$= \prod_{j=1}^{m} \left| \frac{-\beta_j - ck_2/\omega}{-\beta_j - ck_1/\omega} \right|$$

$$= \prod_{j=1}^{m} \left| \frac{-\beta_j + s}{-\beta_j - s} \right|, \tag{2.11}$$

where $s = ck_1/\omega = |ck_2/\omega|$. This is the same as the reflection coefficient (2.9) for the upper layer. As before, the reflection coefficient can be given a geometrical interpretation in terms of ratios of distances.

The reflection coefficients (2.9) and (2.11) are graphed in Fig. 2.3. In each frame, the horizontal coordinate is the scaled horizontal wavenumber, which is the same in both layers. In each case, this quantity is plotted on the bottom axis, and corresponding angles of incidence are plotted on the top axis. In a sense, the reflection coefficients in Fig. 2.3 are plotted as functions of the wave, and the coefficients are the same in both layers.

3. ELASTIC WAVES

Absorbing boundary conditions for elastic waves in homogeneous media are developed and analyzed in [10], and a practical exposition of the main ideas is given in [11]. The goal of the present section is to analyze the performance of these boundary conditions along a vertical computational boundary in a horizontally stratified medium. Elastic waves are more complicated than acoustic waves, and it is not correct to say that the absorption properties of the boundary conditions are independent of the layer. However, these properties do not vary greatly from one layer to another, and the boundary conditions yield good absorption in each layer, even in the presence of strong contrasts between layers.

3.1. Properties of Solutions of the Elastic Wave Equation

For later reference, we summarize some properties of the elastic wave equation. Let D be a domain in R^n ($n = 2$ or 3) that represents the position at equilibrium of an isotropic elastic medium. For any $\mathbf{x} \in D$ and any time t, let $\mathbf{U}(\mathbf{x}, t) \in R^n$ denote the displacement from equilibrium of the material particle whose equilibrium position is $\mathbf{x}$. If the magnitude of $\mathbf{U}$ is small relative to the length scale on which $\mathbf{U}$ and the properties of the medium vary, then

$$\rho \frac{\partial^2 U_i}{\partial t^2} = \frac{\partial}{\partial x_i}(\lambda\theta) + \sum_{j=1}^{n} \frac{\partial}{\partial x_j}\left[\mu\left(\frac{\partial U_i}{\partial x_j} + \frac{\partial U_j}{\partial x_i}\right)\right] \tag{3.1}$$

for $1 \leqslant i \leqslant n$; here $\rho(\mathbf{x})$ is the density of the medium, $\lambda(\mathbf{x})$ and $\mu(\mathbf{x})$ are the Lamé parameters, and $\theta = \sum_{j=1}^{n} \partial U_j/\partial x_j$ (see, e.g., Aki and Richards [1] or Bullen and Bolt [2]).

In later discussions involving layered media, it will be necessary to refer to properties of solutions of (3.1) in homogeneous regions. For definiteness, we consider the case of two dimensions; analogous properties apply to

problems in three dimensions (see [10]). In a two-dimensional uniform medium, (3.1) can be written in the form

$$\rho \begin{pmatrix} u \\ w \end{pmatrix}_{tt} = \begin{pmatrix} \lambda+2\mu & 0 \\ 0 & \mu \end{pmatrix} \begin{pmatrix} u \\ w \end{pmatrix}_{xx} + \begin{pmatrix} \mu & 0 \\ 0 & \lambda+2\mu \end{pmatrix} \begin{pmatrix} u \\ w \end{pmatrix}_{zz} + \begin{pmatrix} 0 & \lambda+\mu \\ \lambda+\mu & 0 \end{pmatrix} \begin{pmatrix} u \\ w \end{pmatrix}_{xz}. \tag{3.2}$$

Here, the spatial variables are denoted by x and z, and the x- and z-displacements are denoted by u and w, respectively. The variable z will be regarded as a vertical coordinate, with positive direction downward. Subscripts in (3.2) denote partial differentiations.

Consider waves of the form

$$e^{ikx+ilz-i\omega t}q, \tag{3.3}$$

where q is a vector having two real components, and k, l, and ω are real scalars. If (3.3) is a solution of (3.2), then the dual variables in (3.3) must satisfy the dispersion relation

$$\omega^2 = c_P^2(k^2+l^2) \tag{3.4a}$$

or

$$\omega^2 = c_S^2(k^2+l^2), \tag{3.4b}$$

where

$$c_P = ((\lambda+2\mu)/\rho)^{1/2}, \qquad c_S = (\mu/\rho)^{1/2}. \tag{3.5}$$

In the first case, one can choose

$$q = (k, l)^{\mathrm{T}}; \tag{3.6a}$$

in the second case,

$$q = (-l, k)^{\mathrm{T}}. \tag{3.6b}$$

The vectors in (3.6) can be scaled to unit length by multiplying by c_P/ω and c_S/ω, respectively. In each case, the group and phase velocities coincide and are equal to $c(ck/\omega, cl/\omega)^{\mathrm{T}}$, where $c = c_P$ or $c = c_S$. Waves travelling into (out of) the domain $x > 0$ correspond to k and ω of same (opposite) signs.

If a wave satisfies (3.4a) and (3.6a), then the displacement is parallel to the velocity vector, and the wave motion consists of compressions and expansions. For waves satisfying (3.4b) and (3.6b), the displacement is perpendicular to the direction of wave propagation, and the wave consists of shearing (rotational) motions.

For most hard rock in the earth, λ and μ are approximately equal (see Bullen and Bolt [2, p. 89]). If $\lambda = \mu$, then (3.5) implies $c_S/c_P = 1/\sqrt{3} \doteq 0.577$. Smaller values of this ratio are found in materials of lower rigidity.

The preceding discussion has been concerned with body waves, which propagate through the interior of an elastic medium. Now suppose that an elastic medium is bounded above by a horizontal free surface. Along such a surface, Rayleigh waves can propagate. These waves can be regarded as particular linear combinations of P- and S-waves that are evanescent in the sense of decaying with depth and propagating horizontally (see, e.g., Aki and Richards [1]). The speed c_R of Rayleigh waves is slightly less than that of propagating S-waves. For example, if $c_S/c_P = 1/\sqrt{3}$, then $c_R \doteq 0.92c_S$.

3.2. Boundary Conditions

The boundary conditions for elastic waves developed in [10] are generalizations of the boundary conditions for acoustic waves discussed earlier. For the moment, consider the case of a homogeneous medium and suppose that the computational domain corresponds to $x > 0$. For problems in either two or three dimensions, the boundary conditions in [10] are obtained by applying the operator

$$B\left(\frac{\partial}{\partial x}, \frac{\partial}{\partial t}\right) = \prod_{j=1}^{m} \left(\beta_j \frac{\partial}{\partial t} - c_P \frac{\partial}{\partial x}\right) \tag{3.7}$$

to each component of the displacement vector at the boundary $x = 0$. Here, β_j is a positive dimensionless constant, for each j. In practice, one would use $m = 2$ or possibly $m = 3$. In principle, the P-wave speed c_P could be replaced by a different wave speed in some of the factors in (3.7); the use of c_P in each factor amounts to a normalization of coefficients and is done solely for notational convenience.

A motivation for (3.7) is the following: Suppose that a combination of P-waves and S-waves is moving toward the computational boundary. In general, each component of displacement can experience each kind of wave, and each wave speed must be taken into account during the derivation and analysis of boundary conditions. If $0 < \beta_j \leqslant 1$, then the jth factor in the operator (3.7) yields perfect absorption of P-waves traveling at angles of incidence $\pm\cos^{-1}\beta_j$. The jth factor might then be regarded as oriented primarily to absorbing P-waves. However, a key idea behind the reflection analysis given later is that this operator still contributes substantially to the absorption of S-waves. A rough description of this idea is that the jth operator can also be regarded as an "S-wave" operator if it is multiplied by c_S/c_P. This operator thus produces exact absorption of S-waves at angles of incidence $\pm\cos^{-1}(\beta_j(c_S/c_P))$. Such angles might not be optimal for absorbing S-waves, but the jth factor definitely helps to absorb such waves. On the other hand, if

β_j is near c_P/c_S, then the jth factor is oriented primarily to the absorption of S-waves, but it still contributes to the absorption of P-waves.

In general, the parameters β_j can be chosen to orient the boundary condition to one type of wave or to reach a compromise between the two. In some of the numerical computations described in Section 5, the second-order ($m = 2$) version of (3.7) was used, with $\beta_1 = 1$ and $\beta_2 = c_P/c_S$. In this case, (3.7) yields exact absorption of P-waves and S-waves at normal incidence to the boundary. The third-order ($m = 3$) version of (3.7) was also used, with $\beta_1 = 1$, β_2 between 1 and c_P/c_S, and $\beta_3 = c_P/c_S$. Numerical experiments have shown that the performance of (3.7) is not very sensitive to the choices of these parameters. For an example, see Test 1 in Section 5.

Now consider the case of a layered medium. For simplicity, suppose that the medium consists of two homogeneous layers separated by a horizontal interface and suppose that the computational boundary is perpendicular to the interface. Let c_P and c_S denote the P-wave and S-wave speeds in the upper layer, and let c'_P and c'_S denote the speeds in the lower layer. In the lower layer, the operator (3.7) can be applied to each component of displacement at the boundary; equivalently, the operator

$$B'\left(\frac{\partial}{\partial x}, \frac{\partial}{\partial t}\right) = \prod_{j=1}^{m} \left(\beta'_j \frac{\partial}{\partial t} - c'_P \frac{\partial}{\partial x}\right) \tag{3.8}$$

can be applied to each component, where $\beta_j/c_P = \beta'_j/c'_P$ for each j. The values of $\beta_1, \ldots, \beta_m$ could be chosen according to the guidelines mentioned above or according to particular information about wave motions in one of the layers. For example, if the lower layer is faster than the upper layer, and if a downgoing cylindrical or spherical P-wave generates head waves along the interface, then one of the factors in (3.7) and (3.8) could be tuned to a normally incident P-wave in the lower layer. This would mean $\beta'_j = 1$ and $\beta_j = c_P/c'_P$. For an example, see Test 3 in Section 5.

3.3. Analysis of Absorption at the Computational Boundary

In this sub-section we calculate reflection coefficients for (3.7) and (3.8) at the computational boundary. For the sake of definiteness, we write the analysis in terms of two-dimensional problems. The calculation for three-dimensional problems is similar to the two-dimensional case.

Suppose that a plane elastic wave (P or S) moves downward through the upper layer and out of the computational domain. When this wave encounters the interface, it can generate reflected P- and S-waves and transmitted P- and S-waves (see Fig. 3.1). The resulting wave system is therefore rather complicated. We wish to analyze the interaction with the computational boundary of each of the waves in this system. When these waves encounter the computational boundary, each can generate a reflected P-wave and a reflected S-wave. In the following analysis, we therefore analyze the following boundary interactions in each layer: outgoing P-wave and incoming P-wave, outgoing P-wave and incoming S-wave, outgoing S-wave and incoming P-wave, and outgoing S-wave and incoming S-wave. In each case, the reflection coefficient can be regarded as the amplitude of the reflected wave due to an incident wave of unit amplitude. No attempt will be made here to calculate the relative amplitudes of the various waves in the system that approaches the boundary. This would be a matter of calculating reflection and transmission coefficients across the interface, and this is done, for example, by Aki and Richards [1].

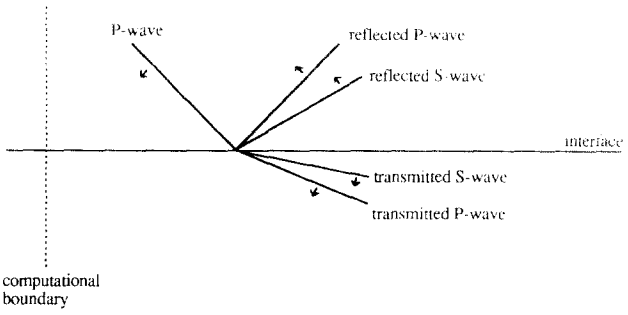

FIG. 3.1. Reflection and transmission of elastic waves at an interface. For each wave, the solid line represents a wave front, and the arrow represents the direction of propagation. In the case illustrated here, the wave velocities in the lower layer are smaller than those in the upper layer.

For the sake of unity in presentation, we write the various reflection coefficients as functions of a quantity that is common to all of the outgoing waves considered here. It is apparent from Fig. 3.1 that angle of incidence is not an appropriate independent variable. Instead, as in the acoustic case, we use a scaled horizontal wavenumber. If the original incident wave in the upper layer has the form $q \exp(ikx + ilz - i\omega t)$, then all of the other waves have the same horizontal wavenumber k and time frequency ω (see, e.g., [1]). For a scaled horizontal wavenumber, we use $c_P k/\omega$. In this definition, the choice of c_P instead of c_S is rather arbitrary; it is done mainly for the sake of notational compatibility with the boundary formula (3.7), which uses c_P.

The dispersion relation (3.4) implies that for waves in the upper layer,

$$\left(\frac{c_P k}{\omega}\right)^2 + \left(\frac{c_P l}{\omega}\right)^2 = 1 \tag{3.9a}$$

for P-waves, and

$$\left(\frac{c_P k}{\omega}\right)^2 + \left(\frac{c_P l}{\omega}\right)^2 = \left(\frac{c_P}{c_S}\right)^2 \tag{3.9b}$$

for S-waves. The scaled horizontal and vertical wavenumbers for oscillatory P- and S-waves therefore lie on circles of radius 1 and $c_P/c_S > 1$, respectively. For waves in the lower layer, the dispersion relation is obtained from (3.4) by replacing c_P and c_S with c'_P and c'_S, respectively. The result can then be written in the form

$$\left(\frac{c_P k}{\omega}\right)^2 + \left(\frac{c_P l}{\omega}\right)^2 = \left(\frac{c_P}{c'_P}\right)^2 \tag{3.10a}$$

for P-waves, and

$$\left(\frac{c_P k}{\omega}\right)^2 + \left(\frac{c_P l}{\omega}\right)^2 = \left(\frac{c_P}{c'_S}\right)^2 \tag{3.10b}$$

for S-waves. The relations (3.9) and (3.10) are graphed in Fig. 3.2. For each kind of wave, the vector from the origin to $(c_P k/\omega, c_P l/\omega)$ gives the direction of propagation in (x, z) space. Waves moving into (out of) the domain $x > 0$ correspond to $c_P k/\omega > 0$ ($c_P k/\omega < 0$).

In the following analysis, the reflection coefficients are written in terms of the quantity $s = |c_P k/\omega|$, where k is the horizontal wavenumber of the outgoing wave under consideration. For P-waves in the upper layer, we have $1 \geqslant s \geqslant 0$. P-waves moving at normal incidence to the boundary $x = 0$ correspond to $s = 1$. For S-waves, we have $c_P/c_S \geqslant s \geqslant 0$. In the lower layer, $c_P/c_S \geqslant s \geqslant 0$ for each type of wave. It is assumed here that the waves in the lower layer are generated by waves moving downward through the upper layer, so the range of possible values of s in the lower layer must coincide with the largest possible range of s in the upper layer. This statement includes the idea that a downgoing S-wave in the upper layer can generate either type of wave in the lower layer. Because of the above condition on s, there may be angles of incidence that cannot actually be seen in the lower layer, or there may be transmitted waves that are not purely oscillatory.

For example, suppose that in Fig. 3.2, the circle for P-waves in the lower layer is larger than the circle for S-waves in the upper layer. In this case, there is a range of directions for P-waves in the lower layer that cannot actually be seen, and there is also a much larger range of directions for S-waves that cannot be seen. This case occurs if and only if $c_P/c'_P > c_P/c_S$, or $c'_S < c'_P < c_S < c_P$. In other words, all waves in the lower layer are slower than all waves in the upper layer. On the other hand, if $c'_P > c_S$, then there is a range of scaled horizontal wavenumbers for S-waves in the upper layer that cannot correspond to oscillatory P-waves in the lower layer. In this case the transmitted P-wave is evanescent, in the sense of propagating horizontally and decaying with depth. Similarly, transmitted evanescent S-waves can also occur, depending on the rela-

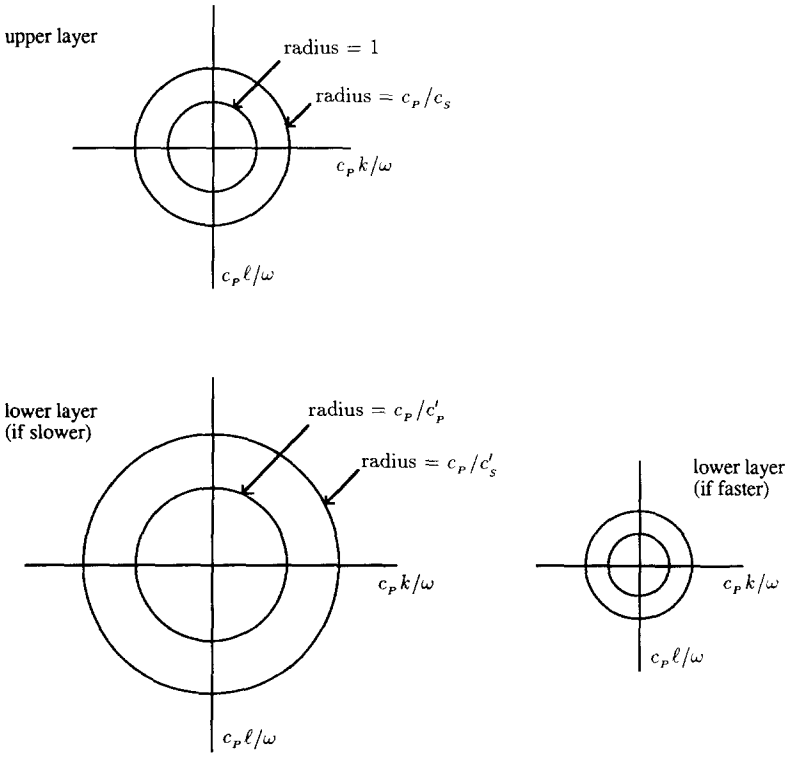

FIG. 3.2. Graphs of scaled wavenumbers for elastic body waves. In each graph, the smaller circle represents the set of all possible scaled wavenumbers for P-waves, and the larger circle represents the possible scaled wavenumbers for S-waves. The velocities in the upper and lower layers are denoted by c_P, c_S and c'_P, c'_S, respectively.

tionships between the velocities in the upper and lower layers.

For reasons given later, the following analysis does not cover the case of transmitted evanescent waves. For the lower layer, the analysis therefore gives a complete description of wave interactions at the computational boundary if $c'_P \leqslant c_S$, and it gives a partial description otherwise. The description of wave interactions in the upper layer is complete, under any circumstances. The empirical results in Section 5 include computations for which $c'_P = 2c_P$, so c'_P is substantially greater than c_S in those computations. The boundary conditions are found to be effective in that case.

coefficients for the upper layer and then translate the results into reflection coefficients for the lower layer.

3.3.1. *Upper Layer*

First consider the reflections generated by an outgoing P-wave in the upper layer. To do this, we assume that a linear combination of the form

$$a_{IP} e^{ik_{IP}x + ilz - i\omega t} q_{IP} + a_{IS} e^{ik_{IS}x + ilz - i\omega t} q_{IS} + a_{OP} e^{ik_{OP}x + ilz - i\omega t} q_{OP} \tag{3.11}$$

satisfies the boundary condition defined by (3.7) at $x = 0$. The first term in (3.11) represents an incoming (reflected) P-wave, the second represents an incoming S-wave, and the third represents an outgoing (incident) P-wave (see Fig. 3.3). The coefficient a_{OP} is assumed to be known, and the goal is to calculate a_{IP} and a_{IS}. For a good absorbing boundary condition, $|a_{IP}/a_{OP}|$ and $|a_{IS}/a_{OP}|$ should be as small as possible.

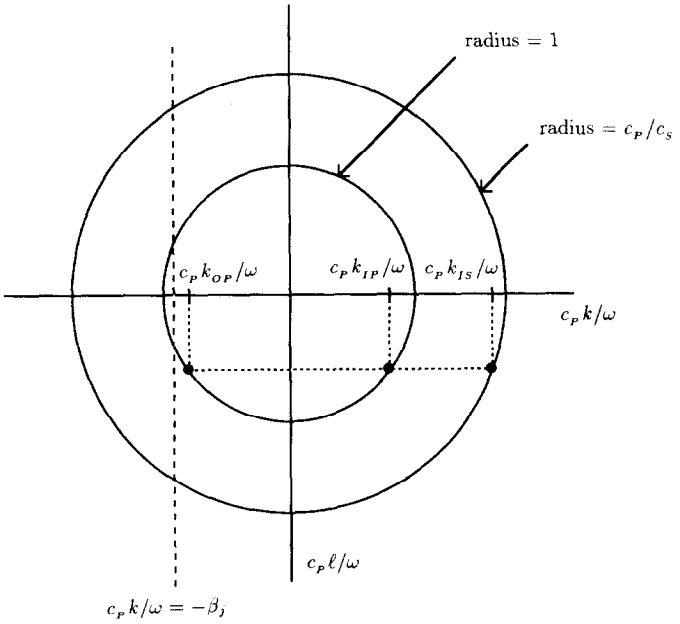

FIG. 3.3. Illustration of the scaled wavenumbers that are involved in the reflection analysis for an outgoing P-wave in the upper layer. Points on the line $c_P k/\omega = -\beta_j$ correspond to outgoing waves that are absorbed exactly by the jth factor in the boundary operator.

The vectors q_{IP}, q_{IS}, and q_{OP} are assumed to be normalized to unit length. Thus, from (3.6),

$$\begin{aligned} q_{IP} &= (c_P k_{IP}/\omega,\ c_P l/\omega)^{\mathrm{T}} \\ q_{IS} &= (-c_S l/\omega,\ c_S k_{IS}/\omega)^{\mathrm{T}} \\ q_{OP} &= (c_P k_{OP}/\omega,\ c_P l/\omega)^{\mathrm{T}}. \end{aligned} \tag{3.12}$$

[redacted]

cancel the factors $\exp(ilz - i\omega t)$. The result is

$$a_{IP} B(ik_{IP}, -i\omega)\, q_{IP} + a_{IS} B(ik_{IS}, -i\omega)\, q_{IS} + a_{OP} B(ik_{OP}, -i\omega)\, q_{OP} = 0$$

or

$$[B(ik_{IP}, -i\omega)\, q_{IP},\ B(ik_{IS}, -i\omega)\, q_{IS}] \begin{pmatrix} a_{IP} \\ a_{IS} \end{pmatrix} = -a_{OP} B(ik_{OP}, -i\omega)\, q_{OP}. \tag{3.13}$$

In (3.13), the bracketed quantity is the square matrix whose columns are the vectors that are shown. Equation (3.13) will be regarded as a linear system with unknowns a_{IP} and a_{IS}.

We first calculate a_{IP}. Cramer's rule yields

$$a_{IP} = \frac{\det[-a_{OP} B(ik_{OP}, -i\omega)\, q_{OP},\ B(ik_{IS}, -i\omega)\, q_{IS}]}{\det[B(ik_{IP}, -i\omega)\, q_{IP},\ B(ik_{IS}, -i\omega)\, q_{IS}]}$$

$$= \frac{B(ik_{OP}, -i\omega)}{B(ik_{IP}, -i\omega)} \left(-\frac{\det[q_{OP}, q_{IS}]}{\det[q_{IP}, q_{IS}]} \right) a_{OP}.$$

In this calculation, we have taken advantage of the fact that the same operator is applied to all components of the displacement vector when the boundary condition is imposed; this leads to *scalar* multiples of the vectors q_{IP}, q_{IS}, and q_{OP}, and these can be factored out in a convenient manner. If different operators were applied to the displacement vector at the boundary, then the above calculation would be more complicated.

The reflection coefficient R_{PP} is defined by

$$|a_{IP}| = R_{PP} |a_{OP}| = R^B_{PP} R^D_{PP} |a_{OP}|, \tag{3.14a}$$

where

$$R^B_{PP} = \left| \frac{B(ik_{OP}, -i\omega)}{B(ik_{IP}, -i\omega)} \right| \tag{3.14b}$$

and

$$R_{PP}^{D} = \left| \frac{\det[q_{OP}, q_{IS}]}{\det[q_{IP}, q_{IS}]} \right|. \tag{3.14c}$$

The factor R_{PP}^{B} represents the effect of the boundary operator $B(\partial/\partial x, \partial/\partial t)$, in a sense, and R_{PP}^{D} is the P-wave-to-P-wave reflection coefficient for the homogeneous Dirichlet boundary condition $u = w = 0$. (To see the latter statement, pretend that B is the identity operator.)

The form (3.7) of the boundary operator implies

$$\begin{aligned} R_{PP}^{B} &= \prod_{j=1}^{m} \left| \frac{\beta_j(-i\omega) - c_P(ik_{OP})}{\beta_j(-i\omega) - c_P(ik_{IP})} \right| \\ &= \prod_{j=1}^{m} \left| \frac{-\beta_j - (c_P k_{OP}/\omega)}{-\beta_j - (c_P k_{IP}/\omega)} \right| \\ &= \prod_{j=1}^{m} \left| \frac{-\beta_j + s}{-\beta_j - s} \right|, \end{aligned} \tag{3.15}$$

where $s = |c_P k_{OP}/\omega| = c_P k_{IP}/\omega$. As in the acoustic case, each factor in (3.15) can be interpreted as a ratio of distances. The numerator in the jth factor is the distance from the line $c_P k/\omega = -\beta_j$ to the point on the smaller circle in Fig. 3.3 having horizontal coordinate $c_P k_{OP}/\omega$; the denominator is the distance from $-\beta_j$ to $c_P k_{IP}/\omega$. The ratio is always less than 1, and it is zero if $-\beta_j = c_P k_{OP}/\omega$.

A calculation involving (3.14c), (3.12), (3.9), and the definition of s yields

$$R_{PP}^{D} = \left| \frac{1 - s^2 - sA}{1 - s^2 + sA} \right|, \tag{3.16}$$

where

$$A = ((c_P/c_S)^2 - 1 + s^2)^{1/2}. \tag{3.17}$$

The reflection coefficient R_{PP} is then given by

$$R_{PP} = \left(\prod_{j=1}^{m} \left| \frac{-\beta_j + s}{-\beta_j - s} \right| \right) R_{PP}^{D}, \tag{3.18}$$

where $1 \geqslant s \geqslant 0$.

We now calculate the coefficient a_{IS} of the incoming S-wave in the linear combination (3.11). When Cramer's rule is applied to the linear system (3.13), the result is

$$a_{IS} = \frac{B(ik_{OP}, -i\omega)}{B(ik_{IS}, -i\omega)} \left(-\frac{\det[q_{IP}, q_{OP}]}{\det[q_{IP}, q_{IS}]} \right) a_{OP}.$$

We then define a reflection coefficient R_{SP} by $|a_{IS}| = R_{SP}\,|a_{OP}| = R_{SP}^{B} R_{SP}^{D}\,|a_{OP}|$, where R_{SP}^{B} and R_{SP}^{D} are defined in a manner analogous to (3.14b)–(3.14c). The first of these is

$$\begin{aligned} R_{SP}^{B} &= \left| \frac{B(ik_{OP}, -i\omega)}{B(ik_{IS}, -i\omega)} \right| \\ &= \prod_{j=1}^{m} \left| \frac{-\beta_j - (c_P k_{OP}/\omega)}{-\beta_j - (c_P k_{IS}/\omega)} \right| \\ &= \prod_{j=1}^{m} \left| \frac{-\beta_j + s}{-\beta_j - A} \right|, \end{aligned} \tag{3.19}$$

where A is defined in (3.17). The definition of s and the relations in (3.9) are used to obtain the last equation in (3.19). As before, R_{SP}^{B} can be interpreted in terms of ratios of distances in Fig. 3.3, and each factor in (3.19) is always less than 1. The reflection coefficient for the Dirichlet boundary condition is

$$\begin{aligned} R_{SP}^{D} &= \left| \frac{\det[q_{IP}, q_{OP}]}{\det[q_{IP}, q_{IS}]} \right| \\ &= \frac{2s(1 - s^2)^{1/2}}{(c_S/c_P)[1 - s^2 + sA]}. \end{aligned}$$

The reflection coefficient R_{SP} is then given by

$$R_{SP} = R_{SP}^{B} R_{SP}^{D} \tag{3.20}$$

for $1 \geqslant s \geqslant 0$.

We next examine the reflections produced by an outgoing S-wave $a_{OS} q_{OS} \exp(ik_{OS}x + ilz - i\omega t)$ in the upper layer. In this case, reflection coefficients are expressed in terms of the quantity $s = |c_P k_{OS}/\omega|$, and $c_P/c_S \geqslant s \geqslant 0$.

The analysis is divided into two cases. If $|c_P l/\omega| \leqslant 1$, then the outgoing S-wave generates a reflected oscillatory P-wave and a reflected oscillatory S-wave. This situation is illustrated in Fig. 3.4. The horizontal line corresponds to the fixed value of $c_P l/\omega$ that is found in the outgoing and incoming waves considered here. The line intersects both circles in the graph. On the other hand, suppose $1 < |c_P l/\omega| \leqslant c_P/c_S$. In this case, a horizontal line for fixed $c_P l/\omega$ intersects the outer circle, which corresponds to oscillatory S-waves, but it does not intersect the inner circle, which corresponds to oscillatory P-waves. An outgoing oscillatory S-wave is thus possible, and it can generate an oscillatory incoming S-wave. However, an oscillatory incoming P-wave is not possible, and instead there can be a reflected evanescent P-wave having the form

$$e^{\kappa_{IP} x + ilz - i\omega t} q_{IP}.$$

Here, κ_{IP} is real, and $\kappa_{IP} < 0$ if the spatial domain is $x > 0$. This mode propagates in the vertical direction and decays in

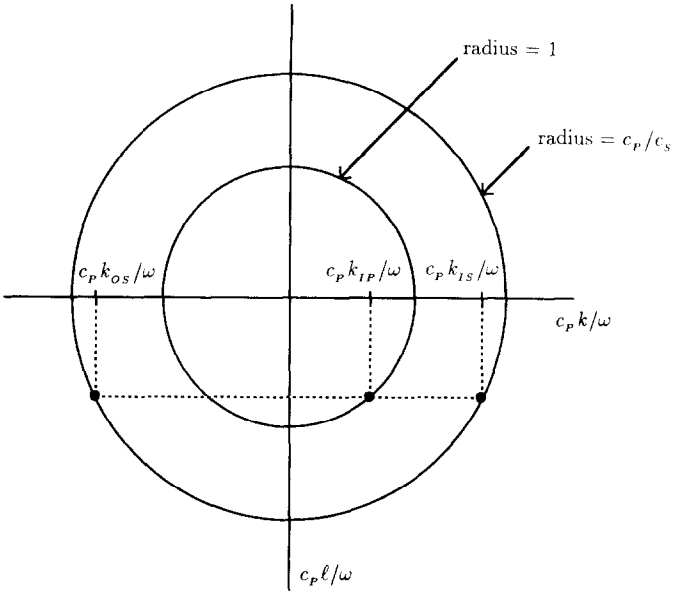

FIG. 3.4. Illustration of the scaled wavenumbers that are involved in the reflection analysis for an outgoing S-wave in the upper layer. In the case shown here, $|c_P l/\omega| \leq 1$, and the reflected P-wave is oscillatory. If $|c_P l/\omega| > 1$, then the reflected P-wave is evanescent.

the inward horizontal direction. The dual variables satisfy $(-i\omega)^2 = c_P^2(\kappa_{IP}^2 + (il)^2)$; this is an analogue of (3.4a). The vector q_{IP} is any scalar multiple of $(\kappa, il)^T$.

Incoming oscillatory P-waves are found if and only if $c_P/c_S \geq s \geq ((c_P/c_S)^2 - 1)^{1/2}$. This condition is obtained by inserting the extreme values $c_P l/\omega = 0$ and $|c_P l/\omega| = 1$ into the relation (3.9b) for scaled wavenumbers for S-waves. Equivalently, one can use Fig. 3.4; s represents the absolute values of horizontal coordinates of points on the larger circle, the vertical coordinate varies from 0 to ± 1, and the radius is c_P/c_S. Evanescent P-waves are found for $((c_P/c_S)^2 - 1)^{1/2} \geq s \geq 0$. If $c_P/c_S = \sqrt{3}$, then an evanescent P-wave is encountered if and only if the outgoing S-wave travels at an angle of incidence greater than $\cos^{-1}(2/3)^{1/2} \doteq 35.26°$.

In order to analyze the reflections produced by the outgoing S-wave, we suppose that a linear combination

$$a_{IP} e^{\kappa_{IP} x + ilz - i\omega t} q_{IP} + a_{IS} e^{ik_{IS} x + ilz - i\omega t} q_{IS} + a_{OS} e^{ik_{OS} x + ilz - i\omega t} q_{OS}$$

satisfies the boundary condition at $x = 0$. If $c_P/c_S \geq s \geq ((c_P/c_S)^2 - 1)^{1/2}$, then $\kappa_{IP} = ik_{IP}$, where k_{IP} is real. Otherwise, κ_{IP} is real and negative. The vectors q_{IP}, q_{IS}, and q_{OS} are assumed to be normalized to unit length. The calculations for this case are analogues of those used in the analysis of an outgoing P-wave, so we only state the final conclusions.

For the incoming P-wave, we define a reflection coefficient R_{PS} by $|a_{IP}| = R_{PS}\,|a_{OS}|$. If the P-wave is purely oscillatory, then

$$R_{PS} = \left(\prod_{j=1}^{m} \left| \frac{-\beta_j - (c_P k_{OS}/\omega)}{-\beta_j - (c_P k_{IP}/\omega)} \right| \right) R_{PS}^D = \left(\prod_{j=1}^{m} \left| \frac{-\beta_j + s}{-\beta_j - E} \right| \right) R_{PS}^D, \tag{3.21a}$$

where

$$R_{PS}^D = \left| \frac{\det[q_{OS}, q_{IS}]}{\det[q_{IP}, q_{IS}]} \right| = \frac{2s(c_S/c_P)\,F^{1/2}}{sE + F}, \tag{3.21b}$$

$$E = (1 - (c_P/c_S)^2 + s^2)^{1/2}, \quad F = (c_P/c_S)^2 - s^2, \tag{3.21c}$$

and $c_P/c_S \geq s \geq ((c_P/c_S)^2 - 1)^{1/2}$. If the incoming P-wave is evanescent, then

$$R_{PS} = \left(\prod_{j=1}^{m} \left| \frac{-\beta_j - (c_P k_{OS}/\omega)}{-\beta_j - (c_P \kappa_{IP}/\omega)(1/i)} \right| \right) R_{PS}^D = \left(\prod_{j=1}^{m} \frac{|-\beta_j + s|}{(\beta_j^2 + F - 1)^{1/2}} \right) R_{PS}^D, \tag{3.22a}$$

where

$$R_{PS}^D = 2s \left(\frac{c_S}{c_P} \right) \left(\frac{F(2F-1)}{F(c_P/c_S)^2 - s^2} \right)^{1/2}, \tag{3.22b}$$

F is defined in (3.21c), and $((c_P/c_S)^2 - 1)^{1/2} \geq s \geq 0$. The mode $q_{IP} \exp(\kappa_{IP} x + ilz - i\omega t)$ decays as x increases, so the effects of this mode are confined to a neighborhood of the boundary. For evanescent P-waves, the size of R_{PS} is less significant than it is when the incoming P-wave is oscillatory (propagating).

For the incoming S-wave, a reflection coefficient R_{SS} is defined by $|a_{IS}| = R_{SS}\,|a_{OS}|$. A calculation shows that

$$R_{SS} = \left(\prod_{j=1}^{m} \left| \frac{-\beta_j - (c_P k_{OS}/\omega)}{-\beta_j - (c_P k_{IS}/\omega)} \right| \right) R_{SS}^D = \left(\prod_{j=1}^{m} \left| \frac{-\beta_j + s}{-\beta_j - s} \right| \right) R_{SS}^D, \tag{3.23a}$$

where $R_{SS}^D = |\det[q_{IP}, q_{OS}]/\det[q_{IP}, q_{IS}]|$. If $c_P/c_S \geq s \geq ((c_P/c_S)^2 - 1)^{1/2}$, then

$$R_{SS}^D = \left| \frac{F - sE}{F + sE} \right|, \tag{3.23b}$$

and if $((c_P/c_S)^2 - 1)^{1/2} \geq s \geq 0$, then $R_{SS}^D = 1$.

The reflection coefficients R_{PP}, R_{SP}, R_{PS}, and R_{SS} given in (3.18), (3.20), (3.21), (3.22), and (3.23) are plotted in

Fig. 3.5. In these graphs, it is assumed that $c_P/c_S = \sqrt{3}$. Graphs are given for $m = 2$ and $m = 3$, with $\beta_1 = 1$, $\beta_2 = \sqrt{3}$, and $\beta_3 = 1.3$. Different choices of parameters would yield different plots. The formulas for the reflection coefficients show that these coefficients are zero if $s = \beta_j$ for some j. The parameters β_1, β_2, and β_3 can therefore be regarded as values of s for which the boundary conditions yield exact absorption.

3.3.2. *Lower Layer*

We now translate the preceding results into reflection

[redacted]

a wave moving downward through the upper layer. All of the waves in this system have the same horizontal wavenumber k and time frequency ω, and all reflection coefficients are written in terms of the common quantity $s = |c_P k/\omega|$. In the lower layer we have $c_P/c_S \geq s \geq 0$, since this is the maximum range of s for waves in the upper layer. In the following discussion, it is assumed that the waves that are transmitted into the lower layer are purely oscillatory (propagating). A few remarks on transmitted evanescent waves are given later.

The conclusions of the analysis can be summarized as follows. As before, each reflection coefficient is written as a product of two factors; one of the factors involves the boundary operator B, and the other is a reflection coefficient for the homogeneous Dirichlet boundary condition. When expressed as a function of s, the first factor is either the same in both layers or nearly the same. On the other hand, the reflection coefficient for the Dirichlet condition is not the same in the two layers, when written in terms of s. Overall, the reflection coefficients for the absorbing boundary conditions are not the same in the two layers. However, they are sufficiently close to each other that it is possible to obtain good absorption in both layers, even in the presence of strong contrasts between layers.

operator (3.7) to each component of displacement in each layer. For the lower layer, we can also think in terms of applying the equivalent operator (3.8),

$$B'\left(\frac{\partial}{\partial x}, \frac{\partial}{\partial t}\right) = \prod_{j=1}^{m} \left(\beta_j' \frac{\partial}{\partial t} - c_P' \frac{\partial}{\partial x}\right),$$

where $\beta_j/c_P = \beta_j'/c_P'$ for all j. The reflection coefficients for the upper layer were concerned with outgoing oscillatory waves. Reflection coefficients for outgoing oscillatory waves in the lower layer can therefore be obtaind from the earlier results by replacing c_P, c_S, β_j, and $s = |c_P k/\omega|$ by c_P', c_S', β_j',

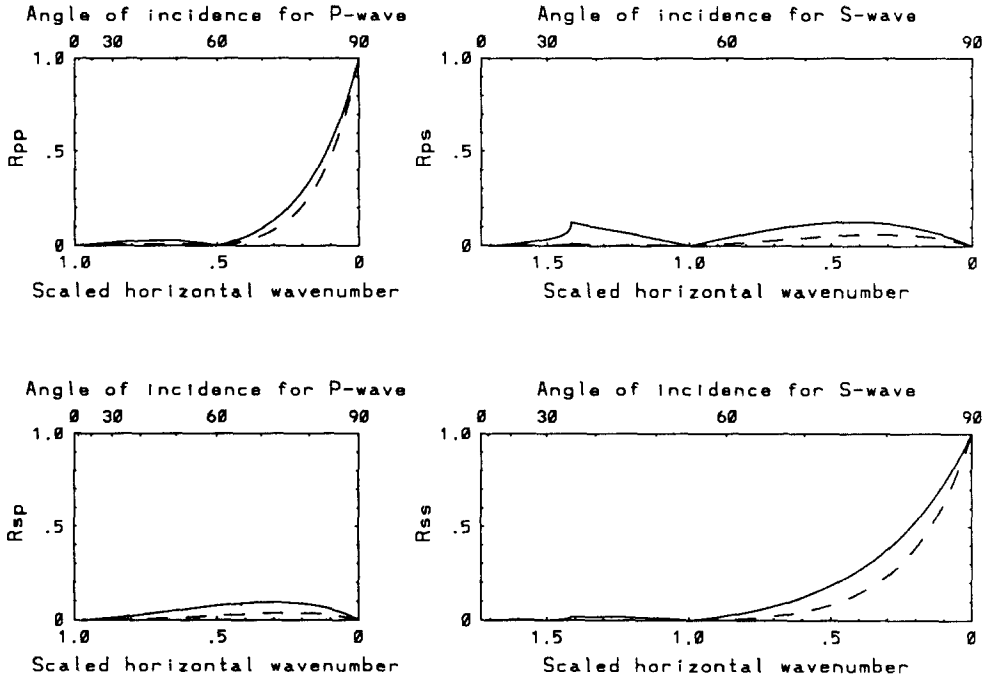

FIG. 3.5. Plots of reflection coefficients at the computational boundary in the upper layer. In each case, the coefficient is plotted as a function of the quantity $s = |c_P k/\omega|$, where k is the horizontal wavenumber of the outgoing wave under consideration. This quantity is invariant under reflection, refraction, and conversion at the interface between the upper and lower layers. The plots show reflection coefficients for second-order ($m = 2$) and third-order ($m = 3$) boundary conditions, with $\beta_1 = 1$, $\beta_2 = c_P/c_S = \sqrt{3}$, and $\beta_3 = 1.3$. The solid curves correspond to $m = 2$, and the dashed curves correspond to $m = 3$. Exact absorption occurs if $s = \beta_1$, β_2, or β_3. R_{PP}: amplitude of the reflected P-wave due to an incident P-wave of unit amplitude. R_{SP}: reflected S-wave, incident P-wave. R_{PS}: reflected P-wave, incident S-wave. R_{SS}: reflected S-wave, incident S-wave.

and $s' = |c'_P k/\omega|$, respectively. These formulas can be written in terms of s by using the relation $s' = (c'_P/c_P)s$, and it is then possible to plot the reflection coefficients and compare them with the reflection coefficients for the upper layer.

Before examining plots, we first analyze some aspects of the reflection coefficients for the lower layer. In order to determine the reflections produced by an outgoing P-wave, we assume that a linear combination

$$a'_{IP} e^{ik'_{IP}x + il'z - i\omega t} q'_{IP} + a'_{IS} e^{ik'_{IS}x + il'z - i\omega t} q'_{IS} + a'_{OP} e^{ik'_{OP}x + il'z - i\omega t} q'_{OP} \tag{3.24}$$

satisfies the boundary condition at $x = 0$. The frequency ω is the same as in the original incident wave (P or S) in the upper layer that generates the wave system that approaches the computational boundary; and $k'_{OP} = k$, where k is the horizontal wavenumber of that incident wave.

For the reflected P-wave, we have $|a'_{IP}| = R'_{PP}\,|a'_{OP}| = R'^{B}_{PP} R'^{D}_{PP}\,|a'_{OP}|$, where

$$R'^{B}_{PP} = \prod_{j=1}^{m} \left| \frac{-\beta'_j - (c'_P k'_{OP}/\omega)}{-\beta'_j - (c'_P k'_{IP}/\omega)} \right|$$

and R'^{D}_{PP} is obtained from R^{D}_{PP} in (3.16) by replacing c_P, c_S, and s by c'_P, c'_S, and s'. The relation $\beta_j/c_P = \beta'_j/c'_P$ implies

$$R'^{B}_{PP} = \prod_{j=1}^{m} \left| \frac{-\beta_j - (c_P k'_{OP}/\omega)}{-\beta_j - (c_P k'_{IP}/\omega)} \right| = \prod_{j=1}^{m} \left| \frac{-\beta_j + s}{-\beta_j - s} \right|, \tag{3.25}$$

since $s = |c_P k'_{OP}/\omega| = |c_P k/\omega|$ and $c_P k'_{OP}/\omega = -c_P k'_{IP}/\omega$. The formula (3.25) for R'^{B}_{PP} is identical to the expression (3.15) for R^{B}_{PP} in the upper layer. For any given wave system, the same values of s are inserted into these two formulas, due to the preservation of frequency and horizontal wavenumber across the interface.

In a sense, the operator B gives the same contribution to the reflection coefficient in both layers. However, if R'^{D}_{PP} is written in terms of s by using the relation $s' = (c'_P/c_P)s$, the result is different from the reflection coefficient R^{D}_{PP} for the upper layer given in (3.16).

For the incoming S-wave in (3.24), we have $|a'_{IS}| = R'_{SP}\,|a'_{OP}| = R'^{B}_{SP} R'^{D}_{SP}\,|a'_{OP}|$, where

$$R'^{B}_{SP} = \prod_{j=1}^{m} \left| \frac{-\beta'_j - (c'_P k'_{OP}/\omega)}{-\beta'_j - (c'_P k'_{IS}/\omega)} \right| = \prod_{j=1}^{m} \left| \frac{-\beta_j - (c_P k'_{OP}/\omega)}{-\beta_j - (c_P k'_{IS}/\omega)} \right|.$$

The definition of s and the relation (3.10) for scaled wavenumbers in the lower layer yield

$$R'^{B}_{SP} = \prod_{j=1}^{m} \left| \frac{-\beta_j + s}{-\beta_j - ((c_P/c'_S)^2 - (c_P/c'_P)^2 + s^2)^{1/2}} \right|.$$

This is not quite the same as the formula for (3.19) for R^{B}_{SP} in the upper layer, but it reduces to (3.19) if $c'_P = c_P$ and $c'_S = c_S$. As in the case described earlier, the reflection coefficients for the Dirichlet boundary condition are not the same in the two layers.

To summarize, we have shown $R^{B}_{PP} = R'^{B}_{PP}$ and $R^{B}_{SP} \neq R'^{B}_{SP}$. The distinction between these two cases can be visualized by re-examining Fig. 3.3, which illustrates the scaled horizontal wavenumbers that are involved in the reflection analysis for an outgoing P-wave in the upper layer. The analogous picture for the lower layer is the same, except that the circles have different radii. R^{B}_{PP} has been interpreted in terms of ratios of distances from $-\beta_j$ to $c_P k_{OP}/\omega$ and $c_P k_{IP}/\omega$. Similarly, R'^{B}_{PP} can be interpreted in terms of distances from $-\beta_j$ to $c_P k'_{OP}/\omega$ and $c_P k'_{IP}/\omega$. But $k'_{OP} = k_{OP}$, due to the preservation of horizontal wavenumber across the interface; and $k'_{IP} = -k'_{OP} = -k_{OP} = k_{IP}$, due to symmetries about $k = 0$. Therefore, $R^{B}_{PP} = R'^{B}_{PP}$. On the other hand, corresponding symmetries are not found in the relationships among k_{OP}, k_{IS}, k'_{OP}, and k'_{IS}, and $R^{B}_{SP} \neq R'^{B}_{SP}$.

Next consider the reflections produced by an outgoing S-wave in the lower layer. In this case, reflection coefficients are written as functions of $s = |c_P k'_{OS}/\omega|$. An analysis similar to the above shows $R^{B}_{PS} \neq R'^{B}_{PS}$. On the other hand,

$$R'^{B}_{SS} = \prod_{j=1}^{m} \left| \frac{-\beta_j - (c_P k'_{OS}/\omega)}{-\beta_j - (c_P k'_{IS}/\omega)} \right| = \prod_{j=1}^{m} \left| \frac{-\beta_j + s}{-\beta_j - s} \right|.$$

A comparison with (3.23a) yields $R^{B}_{SS} = R'^{B}_{SS}$. As before, the reflection coefficients for the Dirichlet condition are not the same in the two layers.

The reflection coefficients R'_{PP}, R'_{SP}, R'_{PS}, and R'_{SS} are graphed in Fig. 3.6. In these plots, it is assumed that $c'_P = c_P/2$ and $c'_P/c'_S = \sqrt{3}$. In the plots for the upper layer shown in Fig. 3.5, it was assumed that $c_P/c_S = \sqrt{3}$; in that case we then have $c'_S = c_S/2$. If the scaled wavenumbers for the two layers are graphed as in Fig. 3.2, then the circles for the upper layer have radii 1 and $\sqrt{3}$, and the circles for the lower layer have radii 2 and $2\sqrt{3}$. All of the transmitted waves in the lower layer must then be purely oscillatory; no evanescent transmitted waves are possible. All of the reflection coefficients are graphed for $c_P/c_S = \sqrt{3} \geq s \geq 0$, for reasons given earlier.

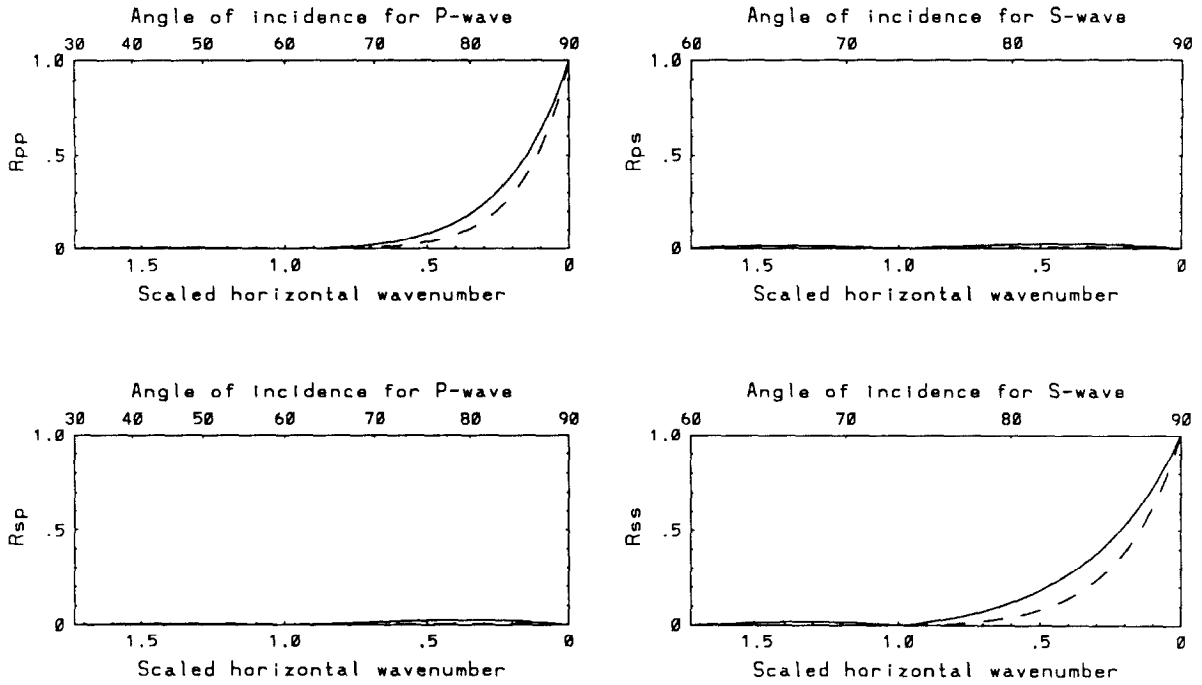

FIG. 3.6. Plots of reflection coefficients for the lower layer. It is assumed that the P-wave and S-wave velocities in the lower layer are equal to one-half the corresponding values for the upper layer. The same values of β_1, β_2, and β_3 are used as in Fig. 3.5. The solid curves correspond to second-order boundary conditions, and the dashed curves correspond to third-order boundary conditions.

The plots show graphs of reflection coefficients for second-order ($m=2$) and third-order ($m=3$) boundary conditions, with $\beta_1=1$, $\beta_2=\sqrt{3}$, and $\beta_3=1.3$. Equivalently, $\beta_1'=1/2$, $\beta_2'=\sqrt{3}/2$, and $\beta_3'=0.65$, since $\beta_j'=(c_P'/c_P)\beta_j=\beta_j/2$ for all j. These are the same choices of parameters as shown in Fig. 3.5 for the upper layer. The graphs shown in Fig. 3.5 and 3.6 are not the same, but the graphs show that good absorption is obtained in each layer.

We conclude with some remarks about transmitted evanescent waves. Conditions for the existence of such waves are discussed before the beginning of Section 3.3.1. Suppose that such a wave (P or S) approaches the computational boundary and denote it by $q\exp(ikx+\gamma z-i\omega t)$, where $\gamma<0$. In order to determine the reflection produced by this wave at $x=0$, one might assume that a linear combination

$$a_{IP}e^{ik_{IP}x+\gamma z-i\omega t}q_{IP}+a_{IS}e^{ik_{IS}x+\gamma z-i\omega t}q_{IS}+e^{ikx+\gamma z-i\omega t}q \tag{3.26}$$

satisfies the boundary condition at $x=0$ in the lower layer. The same dependence with respect to z and t is used so that the boundary condition can be satisfied identically at $x=0$. Reflection coefficients can be calculated in the same manner as before, and the formulas are analogues of ones obtained earlier.

However, there are possible problems with the magnitudes of the reflection coefficients for the Dirichlet boundary condition that are obtained by this process. For example, suppose that the velocities of P- and S-waves in the lower layer are twice as large as those in the upper layer, and suppose $c_P/c_S=c_P'/c_S'=\sqrt{3}$. Reflection coefficients for the lower layer are of interest for $\sqrt{3}\geq s\geq 0$. A horizontally propagating P-wave in the upper layer corresponds to $s=1$, and in this case the analysis yields a value of $R_{PP}^{'D}$ that is approximately equal to 4. The extreme value $s=\sqrt{3}$ corresponds to a horizontally propagating S-wave in the upper layer, and in this case the computed $R_{PP}^{'D}$ is approximately equal to 12. Similar behavior is found in $R_{SP}^{'D}$. It is not clear whether reflection coefficients of this magnitude are physically reasonable, when the homogeneous Dirichlet boundary condition is used. Because of such doubts, details of the above analysis for transmitted evanescent waves are not given here. A possible source of the difficulty is that the linear combination (3.26) might not include a correct formulation of the possible reflected waves.

However, in Test 3 in Section 5, absorbing boundary conditions are tested numerically for the case where the velocities in the lower layer are twice as large as those in the upper layer, and the boundary conditions are found to give effective absorption. In these computations, transmitted evanescent waves are not readily apparent (see Fig. 5.6). This experiment suggests that such waves might not be of significant amplitude, so that propagating waves are of primary concern in the lower layer. The present section gives a complete analysis of that case.

4. NUMERICAL ALGORITHMS

In this section we describe difference approximations to the boundary conditions developed in Sections 2 and 3, and we also describe how to implement these boundary conditions in conjunction with free-surface and interface conditions for elastic waves. The numerical algorithms are stated mainly in terms of two-dimensional problems, and in this case the space domain is assumed to be a rectangle defined by $A \leqslant x \leqslant B$, $0 \leqslant z \leqslant H$, with positive z-direction downward. The difference approximations to absorbing boundary conditions also apply to three-dimensional problems with essentially no modification, and this is also discussed.

4.1. Difference Approximations to Absorbing Boundary Conditions

First consider boundary conditions at $x = A$. For both acoustic and elastic waves, the analytical absorbing boundary conditions fit into the general form

$$B(\partial/\partial x, \partial/\partial t)u = \left[\prod_{j=1}^{m}\left(\beta_j \frac{\partial}{\partial t} - c\frac{\partial}{\partial x}\right)\right]u = 0, \tag{4.1}$$

where the β_j's are positive dimensionless constants. In the acoustic case, c is the wave speed, and u is the dependent variable. In the elastic case, c is replaced by c_P, and the operator B is applied to each component of displacement.

For the sake of deriving difference approximations, let Δx, Δz, and Δt denote the stepsizes in x, z, and t, respectively; and let $u_{J,M}^N$ denote an approximation to a quantity of the form $u(A + J\,\Delta x,\ M\,\Delta z,\ N\,\Delta t)$. Also define shift operators E_x and E_t by

$$E_x u_{J,M}^N = u_{J+1,M}^N, \qquad E_t u_{J,M}^N = u_{J,M}^{N+1}.$$

Then $E_x^{-1}u_{J,M}^N = u_{J-1,M}^N$ and $E_t^{-1}u_{J,M}^N = u_{J,M}^{N-1}$. Assume that the solution has been computed for $t \leqslant N\,\Delta t$, and the solution is then needed at time $t_{N+1} = (N+1)\,\Delta t$. For the sake of definiteness, also assume that the interior scheme yields the solution at time t_{N+1} at the grid points for which $x \geqslant A + \Delta x$, so that the boundary conditions are needed for computing the solution only at the grid points for which $x = A$. This is the case, for example, with standard centered second-order finite difference approximations to the acoustic and elastic wave equations.

An operator $\beta\partial/\partial t - c\partial/\partial x$ can be approximated by

$$D(E_x, E_t^{-1}) = \beta\left(\frac{I - E_t^{-1}}{\Delta t}\right)[(1-b)I + bE_x] - c\left(\frac{E_x - I}{\Delta x}\right)[(1-b)I + bE_t^{-1}], \tag{4.2}$$

where I is the identity operator and b is a constant. In the first term in (4.2), the factor $(I - E_t^{-1})/\Delta t$ represents a backward time difference, and the factor $[(1-b)I + bE_x]$ represents a weighted average in x with weighting coefficients $1-b$ and b. The time differences will be taken with respect to the new time level, so backward time differences are used. The second term in (4.2) represents a forward space difference of a weighted time average. In principle, one could use different pairs of weighting coefficients in the two terms in (4.2); however, the resulting difference operator would be equivalent to an operator of the same form for which the pairs are the same (see Lemma 1 of [9]). Numerical experiments have shown that positive values of b can give slightly better absorption than $b = 0$. The value $b = 0.40$ was used in the numerical computations described in Section 5.

The boundary condition (4.1) can be discretized by

$$\left[\prod_{j=1}^{m} D_j(E_x, E_t^{-1})\right]u_{0,M}^{N+1} = 0, \tag{4.3}$$

where $D_j(E_x, E_t^{-1})$ approximates $\beta_j\partial/\partial t - c\partial/\partial x$. In the formula for D_j, one could choose the weighting coefficient b to depend on j; however, this possibility is not likely to be significant in practice and will not be considered here. To implement (4.3), formally multiply the formulas for the D_j's as polynomials in the symbols E_x and E_t^{-1} and solve for the term that does not contain E_x or E_t^{-1}. That term corresponds to $u_{0,M}^{N+1}$. The other terms correspond to values of u at nearby grid points.

Before the operators $D_j(E_x, E_t^{-1})$ in (4.3) are multiplied together, it is useful to reduce them to a simplified form. A manipulation of (4.2) yields

$$\frac{\Delta t}{(\beta+\nu)(1-b)} D(E_x, E_t^{-1}) = I + q_x E_x + q_t E_t^{-1} + q_{xt} E_x E_t^{-1}, \tag{4.4}$$

where q_x, q_t, and q_{xt} are scalar constants defined by

$$q_x = \frac{b(\beta+\nu) - \nu}{(\beta+\nu)(1-b)}$$

$$q_t = \frac{b(\beta+\nu) - \beta}{(\beta+\nu)(1-b)} \tag{4.5}$$

$$q_{xt} = b/(b-1).$$

Here $\nu = c\,\Delta t/\Delta x$. In practice, one multiplies operators having the form of the right side of (4.4).

We pause for a remark about implementation in layered media. The boundary condition (4.1) can be used in each layer, and in this case the difference approximations are the

same in all layers. On the other hand, consider a medium having two layers and suppose that one prefers to think in terms of the boundary condition

$$\left[\prod_{j=1}^{m}\left(\beta_j'\frac{\partial}{\partial t}-c'\frac{\partial}{\partial x}\right)\right]u=0$$

being used in the lower layer. (In the upper layer, (4.1) is used.) Here, c' is the appropriate velocity in the lower layer, and $\beta_j/\beta_j'=c/c'$ for all j. For the difference approximation to the boundary condition in the lower layer, one obtains (4.4) and (4.5), with β and ν replaced by β' and $\nu'=c'\,\Delta t/\Delta x$, respectively. In particular, one has

$$q_x=\frac{b(\beta'+\nu')-\nu'}{(\beta'+\nu')(1-b)}$$

$$q_t=\frac{b(\beta'+\nu')-\beta'}{(\beta'+\nu')(1-b)}$$

for the lower layer. But the relation $\beta/\beta'=c/c'$ implies that these formulas are the same as in (4.5). The formulas that are actually programmed are thus identical in the two layers.

In the case $m=2$, the boundary condition (4.1) is discretized by using the operator

$$D_1(E_x, E_t^{-1})\,D_2(E_x, E_t^{-1}),$$

where $\beta=\beta_1$ in D_1 and $\beta=\beta_2$ in D_2. Let q_x, q_t, and q_{xt} denote the coefficients of E_x, E_t^{-1}, and $E_xE_t^{-1}$, respectively, in the representation (4.4) of D_1, and let r_x, r_t, and r_{xt} denote the coefficients in the corresponding representation of D_2. The q's are defined by (4.5) with $\beta=\beta_1$; the r's are defined similarly, with $\beta=\beta_2$.

The discrete boundary condition is then

$$\begin{aligned}u_{0,M}^{N+1}&=\gamma_{01}u_{1,M}^{N+1}+\gamma_{02}u_{2,M}^{N+1}\\&\quad+\gamma_{10}u_{0,M}^{N}+\gamma_{11}u_{1,M}^{N}+\gamma_{12}u_{2,M}^{N}\\&\quad+\gamma_{20}u_{0,M}^{N-1}+\gamma_{21}u_{1,M}^{N-1}+\gamma_{22}u_{2,M}^{N-1},\end{aligned}\tag{4.6}$$

where

$$\begin{aligned}\gamma_{01}&=-(q_x+r_x)\\\gamma_{02}&=-q_xr_x\\\gamma_{10}&=-(q_t+r_t)\\\gamma_{11}&=-(q_xr_t+q_tr_x+q_{xt}+r_{xt})\\\gamma_{12}&=-(q_xr_{xt}+r_xq_{xt})\\\gamma_{20}&=-q_tr_t\\\gamma_{21}&=-(q_tr_{xt}+r_tq_{xt})\\\gamma_{22}&=-q_{xt}r_{xt}.\end{aligned}\tag{4.7}$$

In the case of elastic waves, the same difference operator is applied to each component of displacement; for the case of the z-displacement w, just replace each occurrence of the letter "u" in (4.6) with "w."

The notation in (4.6) and (4.7) includes a mechanism for checking for errors in coding. In the term involving γ_{ij} in (4.7), the index i refers to the number of time shifts backward from time level $N+1$. The index i is also equal to the total number of subscripts "t" in each individual term in the formula for γ_{ij} in (4.7). The index j plays a similar role regarding x-shifts and subscripts "x."

Difference approximations to third-order ($m=3$) versions of (4.1) can be obtained in a similar manner. Explicit formulas for this case are given in the Appendix of [11].

Next consider boundary conditions for the boundary segment at $x=B$. For the earlier case, the inward normal direction is the positive x-direction; in the present case, the inward normal direction is the negative x-direction. The reversal of coordinate direction means that the boundary operator is a composition of factors of the form $\beta\partial/\partial t+c\partial/\partial x$, which can be discretized by

$$\begin{aligned}&\beta\left(\frac{I-E_t^{-1}}{\Delta t}\right)[(1-b)I+bE_x^{-1}]\\&\quad+c\left(\frac{I-E_x^{-1}}{\Delta x}\right)[(1-b)I+bE_t^{-1}].\end{aligned}\tag{4.8}$$

In the second term, a backward space difference is used. The difference operator (4.8) has the same form as the earlier difference operator (4.2), except that E_x^{-1} replaces E_x. When operators of the form (4.8) are multiplied together, the same algebraic steps are performed as were done to obtain (4.4)–(4.7), and the final result has the same form as before. The interchange of E_x^{-1} and E_x means that backward space shifts are used instead of forward space shifts. That is, the same formulas are used for both of the boundaries $x=A$ and $x=B$, where in each case the spatial shifts are taken in the inward normal direction.

A similar remark applies to the boundary $z=H$. In this case, the spatial shifts are taken with respect to the z-direction instead of the x-direction.

The above difference formulas also apply to three-dimensional problems. In notations of the form $u_{J,M}^{N}$, an additional index needs to be inserted for the additional coordinate y. However, the boundary conditions still involve shifts only in t and in the inward normal direction, and the boundary conditions have the same form as in two dimensions.

If a value of the solution at a corner of the domain is needed, it can be obtained directly from the boundary condition on one of intersecting boundary segments or planes; just apply the boundary condition right on up to the corner. Before this is done, the solution at neighboring points on the other segment or plane should be computed first.

4.2. Implementation of Free-Surface Conditions for Elastic Waves

We now restrict attention to the case of elastic wave propagation. Suppose that the upper boundary $z=0$ of the computational domain is free to move according to the internal dynamics of the medium. The surface of the earth is an example of such a surface. The freedom of motion can be expressed in terms of certain components of the stress tensor, and these statements then yield physical boundary conditions along the free surface. The numerical implementation of the free-surface conditions at $z=0$ must be coordinated with the implementation of the absorbing boundary conditions along the side boundaries $x=A$ and $x=B$. This issue is typically encountered in the numerical modeling of elastic waves near the surface of the earth, and a free surface is included in the computational models described in Section 5. We therefore discuss these implementation issues in the present sub-section.

The implementation is greatly facilitated by the one-dimensional finite difference stencil of the discrete absorbing boundary conditions that are used here. In the following discussions, most of the work is devoted to implementing the free-surface conditions themselves. Incorporating the absorbing boundary conditions requires relatively little additional effort.

The analysis is stated in terms of two-dimensional problems because the computations described in Section 5 involve two dimensions. For the sake of definiteness, assume that the elastic wave equation is discretized by standard centered second-order finite differences throughout the interior of the domain (see, e.g., Kelly *et al.* [13]).

We first formulate the free-surface conditions for the continuous problem. For a linear, isotropic, two-dimensional elastic medium, the stress tensor is

$$\tau = \begin{pmatrix} \tau_{11} & \tau_{12} \\ \tau_{21} & \tau_{22} \end{pmatrix}$$

$$= \lambda\theta I + 2\mu \begin{pmatrix} u_x & (u_z+w_x)/2 \\ (u_z+w_x)/2 & w_z \end{pmatrix}, \qquad (4.9)$$

where λ and μ are the Lamé parameters, u and w are the x- and z-displacements, $\theta = u_x + w_z$, and I is the identity matrix (see, e.g., Bullen and Bolt [2]). Subscripts on u and w denote partial differentiations. Let (x, z) be any point in the medium, γ a line through (x, z), and $\mathbf{n}$ a unit normal vector to γ through (x, z). The "traction" $\mathbf{T} = \tau\mathbf{n}$ is a vector that represents the force per unit length exerted at (x, z) on the portion of the medium bounded by γ for which $\mathbf{n}$ is the outward normal. At a free surface, the traction must be zero. For the present configuration, $\mathbf{n} = (0, -1)^T$, so the free-surface conditions are $\tau_{12} = 0$ and $\tau_{22} = 0$ at $z = 0$.

More generally, we wish to allow the possibility of external forcing at the free surface; this is how the wave motions are generated in the numerical computations described in Section 5. We therefore implement the physical boundary condition $\tau\mathbf{n} = (P(x, t), Q(x, t))^T$ at $z = 0$. Here, P and Q represent the horizontal and vertical components of the applied force. According to (4.9), this boundary condition is equivalent to

$$\mu(u_z + w_x) = -P(x, t)$$
$$(\lambda + 2\mu)\, w_z + \lambda u_x = -Q(x, t),$$

or

$$\begin{aligned} u_z + w_x &= -p(x, t) \\ w_z + d u_x &= -q(x, t), \end{aligned} \qquad (4.10)$$

where $p = P/\mu$, $q = Q/(\lambda + 2\mu)$, and $d = 1 - 2(c_S/c_P)^2$. The second equation in (4.10) uses the relation $\mu/(\lambda + 2\mu) = (c_S/c_P)^2$, which follows from (3.5). All of the terms in (4.10) are dimensionless.

The first equation in (4.10) can be interpreted in terms of angles of rotation. If $u_z > 0$, then the horizontal displacement u increases with depth. A line which is vertical when the medium is at equilibrium must therefore be rotated counterclockwise. (We assume that the positive x-direction is to the right and the positive z-direction is downward.) Furthermore, $u_z \approx \Delta u/\Delta z$, and this latter quantity approximates the radian measure of the angle of rotation. If $u_z < 0$, then the rotation is clockwise. Similarly, if $w_x > 0$ ($w_x < 0$), then a horizontal line is rotated clockwise (counterclockwise), and w_x approximates the angle of rotation. If $p(x, t) = 0$ in (4.10), then $u_z = -w_x$, and vertical and horizontal lines then experience the same magnitude and direction of rotation.

The second equation in (4.10) involves u_x and w_z. These quantities can be regarded as rates of expansion or compression in the x- and z-directions, respectively. If $q(x, t) = 0$, then u_x and w_z have opposite signs, so a compression in one direction implies an expansion in the other.

We now discuss the implementation of the free-surface conditions in (4.10). Assume that the displacements u and w at time $t_{N+1} = (N+1)\,\Delta t$ have been obtained at all grid points for which $z \geq \Delta z$; these quantities are supplied by the discretization of the elastic wave equation in the interior and the absorbing boundary conditions along the side boundaries $x = A$ and $x = B$. A discretization of (4.10) is then used to obtain displacements at $z = 0$ at time t_{N+1}. This process can be regarded as an evolution in z from $z_1 = \Delta z$ to $z_0 = 0$ for fixed t. Numerical schemes that are explicit in z are straightforward to implement, but such schemes appear to be unstable when the velocity ratio c_S/c_P is sufficiently small (see Vidale and Clayton [22]). Low

values of this ratio are found in materials of relatively low rigidity. We therefore use finite difference approximations to (4.10) that are implicit in z.

Let $x_J = A + J\,\Delta x$, where $\Delta x = (B-A)/L$. The side boundaries are then located at x_0 and x_L. The first equation in (4.10) can be approximated by

$$\frac{\Delta z}{\Delta x}\left(\frac{w^{N+1}_{J+1,1} - w^{N+1}_{J-1,1}}{2\Delta x}\right) + (1-r)\left(\frac{w^{N+1}_{J+1,1} - w^{N+1}_{J-1,1}}{2\Delta x}\right) = -p(x_J, t_{N+1}) \tag{4.11}$$

for $1 \leqslant J \leqslant L-1$. The first term in (4.11) is an approximation to u_z. The second and third terms include approximations to w_x at $z_0 = 0$ and $z_1 = \Delta z$, respectively. A weighted average is then taken of these approximations, with weights r and $1-r$. If $r = \frac{1}{2}$, then (4.11) resembles the Crank–Nicholson method; this discretization of the free-surface condition was used by Vidale and Clayton [22]. If $r = 1$, then (4.11) is a one-sided implicit approximation used by Sochacki *et al.* [20]. If $r = 0$, the method is explicit. The value $r = \frac{1}{2}$ was used in the numerical computations described in Section 5. The second equation in (4.10) can be approximated in a manner similar to (4.11). The difference approximations to (4.10) can also be written in the form

$$\begin{aligned}
u^{N+1}_{J,0} - \frac{r}{2}\left(\frac{\Delta z}{\Delta x}\right)\left[-w^{N+1}_{J-1,0} + w^{N+1}_{J+1,0}\right] &= u^{N+1}_{J,1} + \left(\frac{1-r}{2}\right)\left(\frac{\Delta z}{\Delta x}\right)\left[-w^{N+1}_{J-1,1} + w^{N+1}_{J+1,1}\right] \\
&\quad + (\Delta z)\,p(x_J, t_{N+1}) \\
w^{N+1}_{J,0} - \frac{rd}{2}\left(\frac{\Delta z}{\Delta x}\right)\left[-u^{N+1}_{J-1,0} + u^{N+1}_{J+1,0}\right] &= w^{N+1}_{J,1} + \left(\frac{1-r}{2}\right)d\left(\frac{\Delta z}{\Delta x}\right)\left[-u^{N+1}_{J-1,1} + u^{N+1}_{J+1,1}\right] \\
&\quad + (\Delta z)\,q(x_J, t_{N+1}).
\end{aligned} \tag{4.12}$$

Values of u and w at $z_0 = 0$ appear on the left sides of these equations, and they are regarded as unknown quantities in the present situation. Known quantities at $z_1 = \Delta z$ appear on the right sides.

The equations in (4.12) form a simultaneous system of linear equations that needs to be solved at each time step. The system contains $2L+2$ unknowns, namely, $u^{N+1}_{J,0}$ and $w^{N+1}_{J,0}$ for $0 \leqslant J \leqslant L$. However, there are only $2L-2$ equations, since the difference approximations in (4.11)–(4.12) use centered differences in x and thus are applied at points x_J for which $1 \leqslant J \leqslant L-1$. However, the number of unknowns can be reduced to the number of equations by employing the absorbing boundary conditions along the side boundaries at $x_0 = A$ and $x_L = B$.

Suppose that the absorbing boundary conditions for the left boundary $x = A$ are applied at the upper left corner $(x_0, z_0) = (A, 0)$. Because of the one-dimensional stencil of formulas involve values of u and w along the free surface. The formulas for the first-order ($m = 1$), second-order ($m = 2$), and third-order ($m = 3$) versions of (4.3) can be written in the form

$$\begin{aligned}
u^{N+1}_{0,0} &= g_1 u^{N+1}_{1,0} + g_2 u^{N+1}_{2,0} + g_3 u^{N+1}_{3,0} + g(u, N) \\
w^{N+1}_{0,0} &= g_1 w^{N+1}_{1,0} + g_2 w^{N+1}_{2,0} + g_3 w^{N+1}_{3,0} + g(w, N);
\end{aligned} \tag{4.13}$$

where g_1, g_2, and g_3 are constants; and $g(u, N)$ and $g(w, N)$ are known quantities involving values of u and w, respectively, at $z_0 = 0$ for times $t \leqslant N\,\Delta t$. The first subscript of u and w is the x-index, and the second is the z-index. For first-order boundary conditions, $g_2 = g_3 = 0$. Formulas for second-order boundary conditions are given in (4.6)–(4.7); in this case, $g_1 = \gamma_{01}$, $g_2 = \gamma_{02}$, and $g_3 = 0$.

At the upper right corner $(x_L, z_0) = (B, 0)$, the absorbing boundary conditions of orders three or less can be written in the form

$$\begin{aligned}
u^{N+1}_{L,0} &= h_1 u^{N+1}_{L-1,0} + h_2 u^{N+1}_{L-2,0} + h_3 u^{N+1}_{L-3,0} + h(u, N) \\
w^{N+1}_{L,0} &= h_1 w^{N+1}_{L-1,0} + h_2 w^{N+1}_{L-2,0} + h_3 w^{N+1}_{L-3,0} + h(w, N).
\end{aligned} \tag{4.14}$$

Here, the symbol "h" is used instead of "g" in order to allow for the possibility of different boundary conditions being used at $x = A$ and $x = B$.

The formulas in (4.13)–(4.14) can be used to eliminate the unknowns at the corner points from the linear system in (4.12), and the number of unknowns then equals the number of equations. The resulting linear system can be stated in matrix form as follows: Let

$$\mathbf{u}_0 = (u^{N+1}_{1,0}, u^{N+1}_{2,0}, \ldots, u^{N+1}_{L-1,0})^{\mathrm{T}}$$
$$\mathbf{w}_0 = (w^{N+1}_{1,0}, w^{N+1}_{2,0}, \ldots, w^{N+1}_{L-1,0})^{\mathrm{T}},$$

and let $\mathbf{u}_1$ and $\mathbf{w}_1$ denote the analogous quantities at $z = z_1$. The vectors $\mathbf{u}_0$ and $\mathbf{w}_0$ contain the unknowns in the system. Let B be the $(L-1)\times(L-1)$ tridiagonal matrix having zeros on the main diagonal, -1's along the subdiagonal, and 1's along the superdiagonal. Let G denote the $(L-1)\times(L-1)$ matrix in which the first row is $[-g_1, -g_2, -g_3, 0, 0, \ldots, 0]$, the last row is

$[0, 0, ..., 0, h_3, h_2, h_1]$, and all other entries are zero. The linear system defined by (4.12)–(4.14) can then be written in the form

$$\begin{aligned} \mathbf{u}_0 - \frac{r}{2}\left(\frac{\Delta z}{\Delta x}\right)[B+G]\,\mathbf{w}_0 &= \mathbf{b}_u \\ \mathbf{w}_0 - \frac{rd}{2}\left(\frac{\Delta z}{\Delta x}\right)[B+G]\,\mathbf{u}_0 &= \mathbf{b}_w, \end{aligned} \tag{4.15}$$

where

$$\begin{aligned} \mathbf{b}_u = \mathbf{u}_1 &+ \left(\frac{1-r}{2}\right)\left(\frac{\Delta z}{\Delta x}\right) B\mathbf{w}_1 \\ &+ \frac{r}{2}\left(\frac{\Delta z}{\Delta x}\right)\begin{pmatrix} -g(w, N) \\ 0 \\ \vdots \\ 0 \\ h(w, N) \end{pmatrix} \\ &+ \left(\frac{1-r}{2}\right)\left(\frac{\Delta z}{\Delta x}\right)\begin{pmatrix} -w_{0,1}^{N+1} \\ 0 \\ \vdots \\ 0 \\ w_{L,1}^{N+1} \end{pmatrix} \\ &+ \Delta z \begin{pmatrix} p(x_1, t_{N+1}) \\ p(x_2, t_{N+1}) \\ \vdots \\ p(x_{L-1}, t_{N+1}) \end{pmatrix}. \end{aligned} \tag{4.16}$$

The vector $\mathbf{b}_w$ can be obtained from $\mathbf{b}_u$ by interchanging the roles of the symbols "u" and "w," replacing p with q, and inserting a factor d in each term that involves the ratio $\Delta z/\Delta x$. The above formulation of the linear system is related to one used by Vidale and Clayton [22]; a main difference is that the formulation in [22] does not incorporate the effects of absorbing boundary conditions into the linear system.

The system (4.15) could be written as a $(2L-2)\times(2L-2)$ linear system with solution vector $(\mathbf{u}_0^{\mathrm{T}}, \mathbf{w}_0^{\mathrm{T}})^{\mathrm{T}}$. However, it is more convenient to use the special structure of (4.15) to eliminate either $\mathbf{u}_0$ or $\mathbf{w}_0$ and then solve a system of dimension $(L-1)\times(L-1)$. For example, one can solve for $\mathbf{w}_0$ in the second equation in (4.15) and insert the result into the first equation to obtain

$$\begin{aligned} &\left[I - d\left(\frac{r}{2}\right)^2\left(\frac{\Delta z}{\Delta x}\right)^2[B+G]^2\right]\mathbf{u}_0 \\ &\quad = \mathbf{b}_u + \left(\frac{r}{2}\right)\left(\frac{\Delta z}{\Delta x}\right)[B+G]\,\mathbf{b}_w. \end{aligned} \tag{4.17}$$

The matrix B is tridiagonal. The matrix G is tridiagonal if the absorbing boundary conditions are of order 2 or less, and G is pentadiagonal if the absorbing boundary conditions have order 3. The matrix $(B+G)^2$ therefore has at most four nonzero diagonal bands above the main diagonal and at most four nonzero bands below the main diagonal. The coefficient matrix in (4.17) can therefore be factored and stored efficiently. Once $\mathbf{u}_0$ is calculated, the result can be inserted into the second equation in (4.15) to yield an explicit formula for $\mathbf{w}_0$. The computation of $\mathbf{w}_0$ does not require the solution of a linear system.

The above process yields the values of u and w at all grid points on the free surface, except those at the corner points $(x_0, z_0) = (A, 0)$ and $(x_L, z_0) = (B, 0)$. The corner values can now be calculated explicitly using the absorbing boundary conditions given in (4.13) and (4.14).

4.3. Implementation of Interface Conditions for Elastic Waves

Now consider an elastic medium consisting of homogeneous layers separated by parallel horizontal interfaces. Across each interface, some or all of the material parameters ρ, λ, and μ in (3.1) are discontinuous, and these discontinuities can then yield discontinuities in the wave speeds c_P and c_S. One method of handling the variation in the medium is to apply the constant-coefficient version of the elastic wave equation in each homogeneous region and then connect these regions by implementing physical boundary conditions across each interface. An alternative is to discretize the variable-coefficient version (3.1) of the elastic wave equation and apply it throughout the entire computational domain. Kelly *et al.* [13] state that this gives good results when interfaces are present. However, in some of the numerical computations described in Section 5, there are extreme contrasts between adjacent layers. Instead of applying the variable-coefficient equation across such strong discontinuities, we used the first approach described above. In the present sub-section, we describe how the interface conditions were implemented in those computations. The method is very similar to that developed in Section 4.2 for a free surface, so that interfaces and a free surface can be handled in a unified manner when writing computer programs. In particular, the absorbing boundary conditions along the side boundaries are incorporated into the algorithm in the same manner as before.

As in Section 4.2, the analysis is stated in terms of two-dimensional problems, and the computational domain is a rectangle defined by $A \leqslant x \leqslant B$ and $0 \leqslant z \leqslant H$. A free surface is assumed to be located at the upper boundary $z = 0$. Also suppose that a horizontal interface is located at $z = Z > 0$. In the layer immediately above the interface, let ρ, λ, and μ denote the material parameters, τ denote the stress tensor, c_P and c_S denote the wave speeds, and u and w denote

the horizontal and vertical displacements. Denote the corresponding quantities in the lower layer by ρ', λ', μ', τ', c'_P, c'_S, u', and w', respectively.

The interface conditions for the continuous problem can be described as follows. First, the two layers are assumed to be in welded contact, so the components of displacement must be continuous across the interface. Thus

$$u = u', \qquad w = w' \qquad \text{at} \quad z = Z. \tag{4.18a}$$

Second, let $\mathbf{n} = (0, -1)^T$. The tractions in the two layers must satisfy $\tau\mathbf{n} + \tau'(-\mathbf{n}) = \mathbf{0}$ at the interface. A comparison with (4.9) yields

$$\begin{aligned} \mu(u_z + w_x) &= \mu'(u'_z + w'_x) \\ (\lambda + 2\mu)\, w_z + \lambda u_x &= (\lambda' + 2\mu')\, w'_z + \lambda' u'_x \end{aligned} \tag{4.18b}$$

at $z = Z$.

We now describe a method for implementing the conditions (4.18) numerically. The method uses an approximation to (4.18b) that is implicit in z, and the resulting algorithm is a generalization of an explicit method used by Kelly *et al.* [13].

The method uses overlapping grids for two adjacent layers. At an interface, introduce an extra horizontal row of grid points, so that the lower two grid rows for the upper layer refer to the same positions in space as the upper two grid rows for the lower layer. For example, suppose that the upper layer corresponds to $z \leqslant z_M$, and suppose that the extra grid row is located at $z = z_{M-1}$ and is associated with the lower layer. The lower layer thus corresponds to $z \geqslant z_{M-1}$. We can then formulate difference approximations to (4.18b) that involve values of the solution at z_M and z_{M-1}. Because of the overlapping grids for the two layers, the difference approximations to each side of each equation

Suppose that the solution is known at time $t_N = N\,\Delta t$ throughout the computational domain. The solution at time t_{N+1} can then be computed as follows. In a vicinity of the interface discussed above, the solutions for $z < z_M$ and $z > z_M$ can be computed by using the elastic wave equation in the upper and lower layers, respectively. In order to compute the solution at $z = z_M$, use the elastic wave equation for the lower layer; the solution at time t_N along the extra grid row is used at this stage. The displacements computed at z_M can then be regarded as displacements for the lower layer. However, they are stored in the rectangular arrays mentioned above; and during the computation for the following time level, these values will be used in the computations for both the upper and lower layers. Because of this storage arrangement, the displacements computed at z_M are also regarded as displacements for the upper layer. The conditions in (4.18a), which specify continuity of displacements across the interface, are therefore satisfied implicitly.

There still remains the task of computing solutions at the extra row of grid points for time t_{N+1}; for this we use the stress conditions in (4.18b). These can be written as

$$\begin{aligned} u'_z + w'_x &= \left(\frac{\rho}{\rho'}\right)\left(\frac{c_S}{c'_S}\right)^2 (u_z + w_x) \\ w'_z + (1 - 2(c'_S/c'_P)^2)\, u'_x & \\ &= \left(\frac{\rho}{\rho'}\right)\left(\frac{c_P}{c'_P}\right)^2 [w_z + (1 - 2(c_S/c_P)^2)\, u_x]. \end{aligned} \tag{4.19}$$

These conditions use the relations $\mu = \rho c_S^2$ and $\lambda + 2\mu = \rho c_P^2$, which follow from (3.5). The stress conditions in (4.19) have the same form as the forced free-surface conditions in (4.10), and the stresses on the right sides of (4.19) can then be regarded as forcing terms acting on the lower layer. Because of this similarity, the implementation of (4.19) is very similar to that of (4.10). The derivatives on the left sides of (4.19) can be approximated by finite differences in a manner similar to (4.11). The right sides can also be approximated by finite differences, and the resulting approximations play a role analogous to that of p and q in (4.11)–(4.12).

In the method described above, the extra row of grid points is located at z_{M-1} and is associated with the lower layer. This choice is rather arbitrary. One could also locate the extra row at z_{M+1} and associate it with the upper layer. The upper and lower layers would then correspond to

similar to the ones developed earlier, and we omit the details.

5. NUMERICAL COMPUTATIONS INVOLVING ELASTIC WAVES

The absorbing boundary conditions developed in this paper are now applied to some test problems involving elastic waves. In all of the tests, the computational domain is a two-dimensional region having the form $0 \leqslant x \leqslant B$,

$0 \leqslant z \leqslant H$. A free surface is located at $z = 0$, and waves are generated by external forcing at this boundary. Absorbing boundary conditions are applied along the other boundary segments. The absorbing boundary conditions are found to give effective absorption of P-waves and S-waves propagating through the interior of the medium. At the side boundaries, they also are effective in absorbing Rayleigh waves that propagate along the free surface $z = 0$.

Three series of computations are described here. In these tests, the media have the following configurations:

(1) Uniform medium.

(2) Layered medium, with waves moving downward into slower layers. In the slower layers, the velocity ratio c_S/c_P is very low.

(3) Layered medium, with waves moving downward into a faster layer. The wave system includes head waves moving along the interface.

In the second and third tests, there are strong velocity contrasts between adjacent layers.

The forced free-surface conditions have the form (4.10), where $p(x, t) = 0$ for all (x, t),

$$q(x, t) = \cos^2\left(\frac{\pi(x - C)}{2J_0\,\Delta x}\right) \times \cos^2\left(\frac{\pi(t - (N_0 + 1)\,\Delta t)}{2N_0\,\Delta t}\right) \qquad (5.1)$$

when $|x - C| \leqslant J_0\,\Delta x$ and $|t - (N_0 + 1)\,\Delta t| \leqslant N_0\,\Delta t$, and $q(x, t) = 0$ otherwise. The source term $q(x, t)$ is a smooth function that is centered in space at $x = C$ and has duration $2J_0\,\Delta x$ and $2N_0\,\Delta t$ in x and t, respectively. The horizontal component of the applied force is zero, and the vertical component is positive when it is nonzero. The applied force is therefore a downward push at $z = 0$, and it has finite extent in x and t. At time $t = 0$, the displacements and their first-order time derivatives are assumed to be zero throughout the computational domain.

In order to determine the effectiveness of the absorbing boundary conditions, we compute exact (reflectionless) solutions and compare them with the solutions computed with absorbing boundary conditions. The reflectionless solutions are computed on domains that are much larger than the domain $0 \leqslant x \leqslant B$, $0 \leqslant z \leqslant H$; for these computations, the computational boundaries are chosen so that reflections from those boundaries cannot reach the domain $0 \leqslant x \leqslant B$, $0 \leqslant z \leqslant H$ during the time interval on which the solutions are computed. These solutions are then restricted to $0 \leqslant x \leqslant B$, $0 \leqslant z \leqslant H$. In the following discussions, solutions are compared by plotting graphs and by calculating the quantity

$$((u - u_e)^2 + (w - w_e)^2)^{1/2} \qquad (5.2)$$

at each grid point in (x, z) for various fixed times. Here, (u, w) denotes the solution computed with absorbing boundary conditions, and (u_e, w_e) is the exact (reflectionless) solution; (5.2) is thus the length of the error vector. Discrete L^2 norms (in (x, z)) of functions of the form (5.2) are then used as a measure of the accuracy of (u, w) as an approximation to (u_e, w_e).

In these computations, the elastic wave equation is approximated by standard centered second-order finite differences (see, e.g., Kelly *et al.* [13]). The absorbing boundary conditions, free-surface conditions, and interface conditions are implemented in the manner described in Section 4. Dimensionless space and time coordinates are used throughout these tests.

Test 1. *Uniform medium.* We first consider waves propagating through a homogeneous medium. In this test, the computational domain is defined by $0 \leqslant x \leqslant 2$ and $0 \leqslant z \leqslant 3$. The forcing function (5.1) is centered at $x = 1$, its width in x is eight grid intervals, and its duration in time is 12 time steps. The wave speeds are $c_P = 1$ and $c_S = 1/\sqrt{3} \doteq 0.577$; the grid spacings are $\Delta x = \Delta z = \frac{1}{40}$, and the Courant number is $c_P\,\Delta t/\Delta x = 0.80$. The value of the last parameter guarantees that the interior difference equation satisfies the von Neumann stability condition (see, e.g., Aki and Richards [1]).

Solutions computed with various boundary conditions are plotted in Figs. 5.1, 5.2, and 5.3. Horizontal displacements are shown in the graphs on the left sides of the figures, and vertical displacements are shown on the right. Each curve represents the values of a quantity (i.e., horizontal or vertical displacement) along a vertical line through the medium. At points where a curve lies to the left of its equilibrium position, a negative value is plotted; if a curve lies to the right of equilibrium, a positive value is plotted. In plots of horizontal displacement, the wiggles in the graph can be interpreted literally as displacements in the medium; negative displacements represent leftward movement, and positive displacements represent rightward movement. In plots of vertical displacement, a positive displacement represents a downward movement, and a negative displacement represents an upward movement. For the sake of visibility, the displacements were multiplied by a factor of 10 when these graphs were plotted. In order to keep the curves from being too crowded, the displacements were plotted at every other grid point in x.

The exact solution at times $t = 1.5$ and $t = 2.5$ is shown with solid curves in Fig. 5.1. Solutions using absorbing boundary conditions are also plotted with dashed lines in that figure; these will be discussed later. The figure shows two different waves that are moving downward through the medium. The leading wave is a P-wave, and the trailing wave is an S-wave. By checking signs of displacements, one can verify that the particle displacements are parallel to the

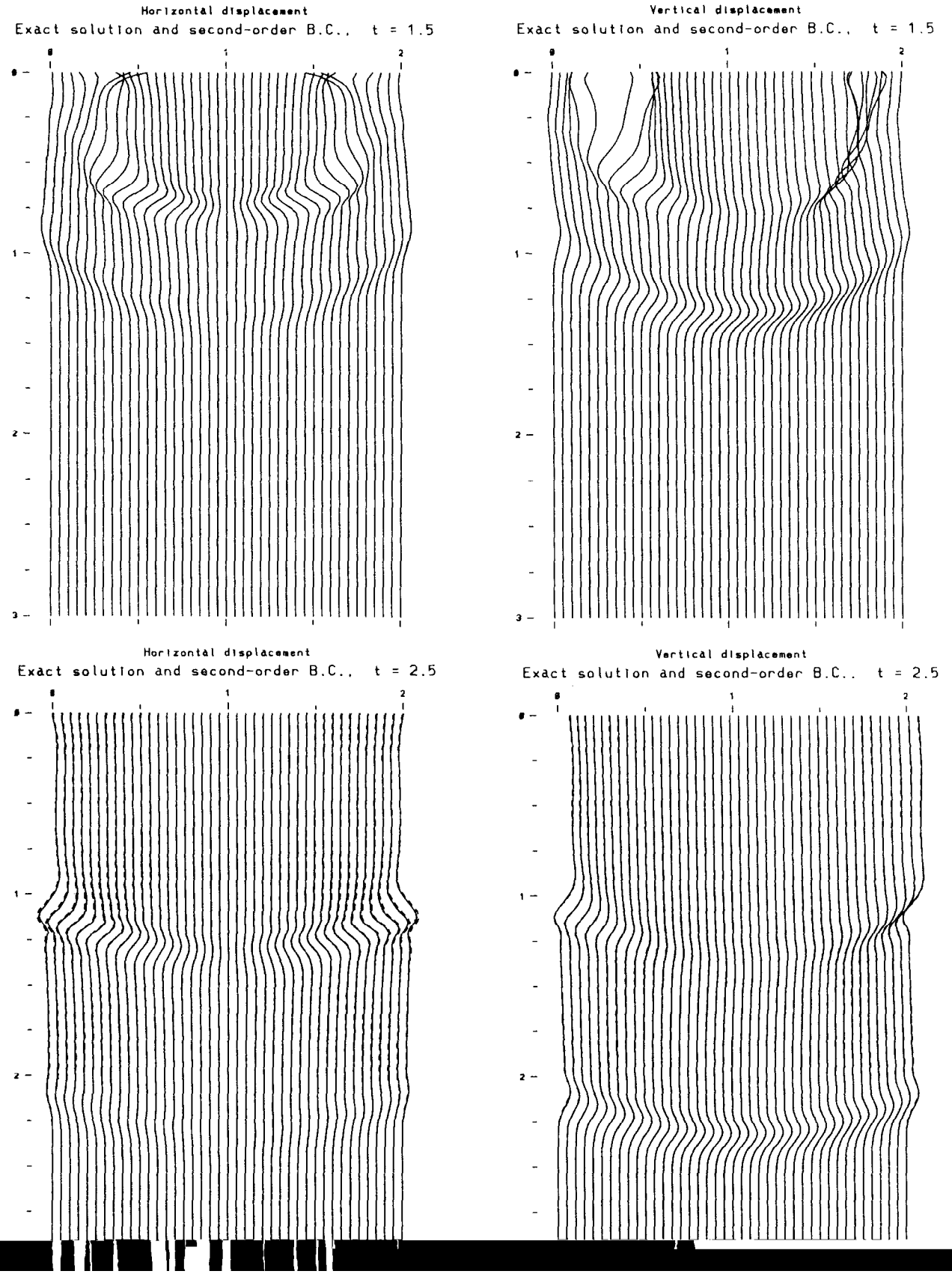

FIG. 5.1. Test 1. Uniform medium. The solid curves show the exact (reflectionless) solution that is obtained by computing on a much larger region. The dashed curves show the solution obtained with the second-order ($m=2$) absorbing boundary condition, with $\beta_1=1$ and $\beta_2=c_P/c_S=\sqrt{3}$. This choice of parameters yields exact absorption of P-waves and S-waves traveling at normal incidence. However, along the side boundaries, these waves are not close to normal incidence. This figure illustrates that the performance of the boundary conditions is not sensitive to the choice of parameters.

direction of propagation in the case of the P-wave, and they are perpendicular to the direction of propagation in the case of the S-wave. The source term used here also excites strong Rayleigh waves moving along the free surface. These are visible at time $t = 1.5$. The Rayleigh waves are moving outward, and by time $t = 2.5$ they have left the domain that is shown here.

Figure 5.2 shows the solution that is obtained when the homogeneous Dirichlet boundary condition $u = w = 0$ is used along the side and bottom boundaries. This boundary condition is totally incompatible with the solution that is sought, and the incompatibility generates strong reflections back into the interior. For example, in the P-wave that is moving downward and outward, the vertical displacements are positive. However, the displacements are required to be zero at the side boundaries. Since the given P-wave does not satisfy this constraint, something else has to be included in the solution so that the superposition does satisfy the boundary condition. This is the cause of the reflection; near each side boundary, one can see an incoming wave having a negative vertical displacement, and the superposition equals zero at the boundary. Similarly, the S-wave and Rayleigh waves generate strong reflections from the computational boundary. The reflected waves then propagate throughout the computational domain and destroy the validity of the solution that is computed there.

The dashed curves in Fig. 5.1 illustrate the solution that is obtained with the second-order ($m = 2$) version of the boundary operator (3.7), with $\beta_1 = 1$ and $\beta_2 = c_P/c_S = \sqrt{3} \doteq 1.732$. This solution agrees closely with the exact solution. On portions of curves where dashed lines are not visible, the two solutions agree to within the width of the plotter lines. Because of the choices of the parameters β_1 and β_2, the boundary condition yields exact absorption of P-waves and S-waves travelling at normal incidence to the boundary. However, the downgoing P- and S-waves are travelling in directions that are far from normal incidence at the side boundaries. This illustrates comments made in earlier sections about the boundary conditions not being sensitive to the choices of parameters.

The plots also show that the outgoing Rayleigh waves are absorbed effectively. This is due to the fact that the speed of Rayleigh waves is close to that of S-waves; when $c_S/c_P = 1/\sqrt{3}$, $c_R \doteq 0.92 c_S$. Because of this situation, the first-order factor in (3.7) that yields exact absorption of normally incident S-waves also yields high absorption of Rayleigh waves.

The amount of reflection at time $t = 1.5$, as measured by the discrete L^2 norm of (5.2), is approximately 2.1% of the L^2 reflection generated by the Dirichlet boundary condition. At time $t = 2.5$, the reflection is 6.8%. At time $t = 5.0$, the reflection is 9.6%.

Figure 5.3 shows the exact solution and the solution computed with the third-order ($m = 3$) version of the boundary operator (3.7), with $\beta_1 = 1$, $\beta_2 = \sqrt{3}$, and $\beta_3 = 1.3$. The agreement between the two solutions is a little closer than in Fig. 5.1. The L^2 reflections are 0.4% at time $t = 1.5$, 2.9% at $t = 2.5$, and 10.5% at $t = 5.0$.

An additional test was performed with a variable-angle second-order boundary condition in which the boundary operator (3.7) at each point on the side boundaries was tuned to waves moving from the source point. The parameters β_1 and β_2 were thus functions of z. One factor in (3.7) was tuned to P-waves, and the other was tuned to S-waves. The results were not quite as good as with the constant-coefficient boundary conditions used above. The L^2 reflections were 2.2% at time $t = 1.5$, 8.7% at $t = 2.5$, and 15.5% at $t = 5.0$.

Test 2. Layered medium, with waves moving downward into slower layers. In this test, the computational domain is defined by $0 \leqslant x \leqslant 2$ and $0 \leqslant z \leqslant 3$, and the medium consists of five homogeneous layers separated by horizontal interfaces. In the top, third, and fifth layers, $c_P = 1$ and $c_S/c_P = 1/\sqrt{3} \doteq 0.577$. In the second and fourth layers, $c_P = 0.5$ and $c_S/c_P = 0.10$. Except for the two slow layers, the medium is the same as in Test 1. The interfaces between the layers are located at $z = 1$, $z = 1.5$, $z = 2$, and $z = 2.5$. The density of the medium is the same in all layers.

The low value of c_S/c_P in the second and fourth layers was chosen in order to illustrate a stability property of the absorbing boundary conditions. According to some empirical studies [4, 17], various earlier absorbing boundary conditions may be unstable if the velocity ratio is sufficiently low. A typical threshold for instability appears to be in the range 0.42–0.46. The value $1/\sqrt{3}$ is approximately equal to common ratios for hard rock in the earth, and lower values [illegible] below the stability threshold are found in some materials of physical interest, including some that are encountered in seismic petroleum exploration. Further discussion of this issue is given in [10]. The value $c_S/c_P = 0.10$ was chosen for the present computations in order to give a severe test of the boundary conditions discussed in the present paper. In [10], the stability of these boundary conditions is analyzed for the case of a homogeneous medium, and the boundary conditions are shown to satisfy the stability criterion of Kreiss [15] for arbitrary values of the velocity ratio. The present numerical experiment suggests stability in the case of a layered medium. Stable behavior and effective absorption were also observed when the limiting value $c_S/c_P = 0$ was used in the two slow layers. However, the solutions for that case are not shown here because the computational model used in this paper is not physically reasonable in that case. If $c_S/c_P = 0$, then $\mu = 0$; the medium in such a layer is an inviscid fluid, and at an interface it is not realistic to require continuity of tangential displacements as in (4.18a).

In these tests, the grid spacings are $\Delta x = \Delta z = \frac{1}{80}$, and the

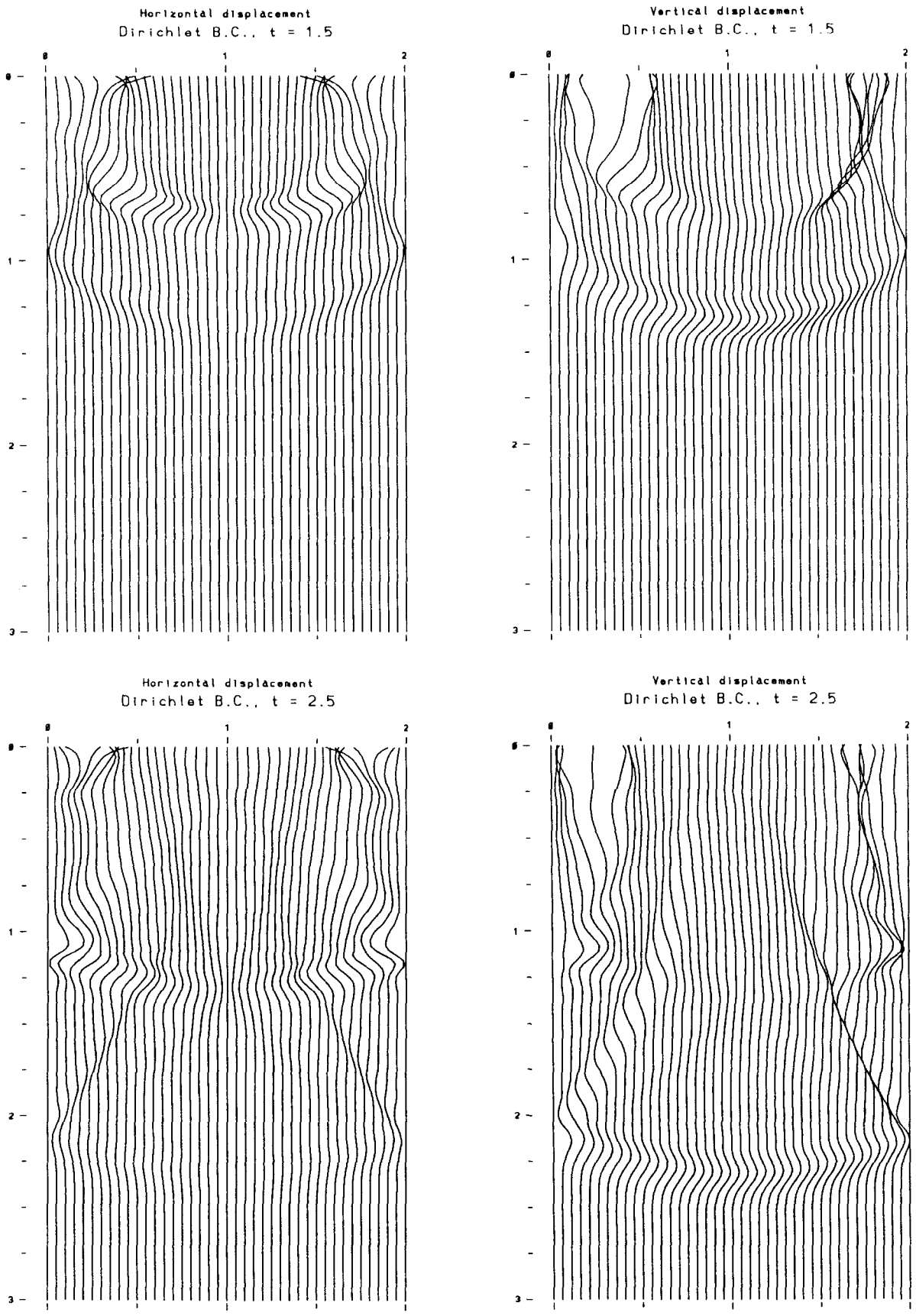

FIG. 5.2. Test 1. Solution obtained with the homogeneous Dirichlet boundary condition $u = w = 0$. Strong reflections are present in this solution.

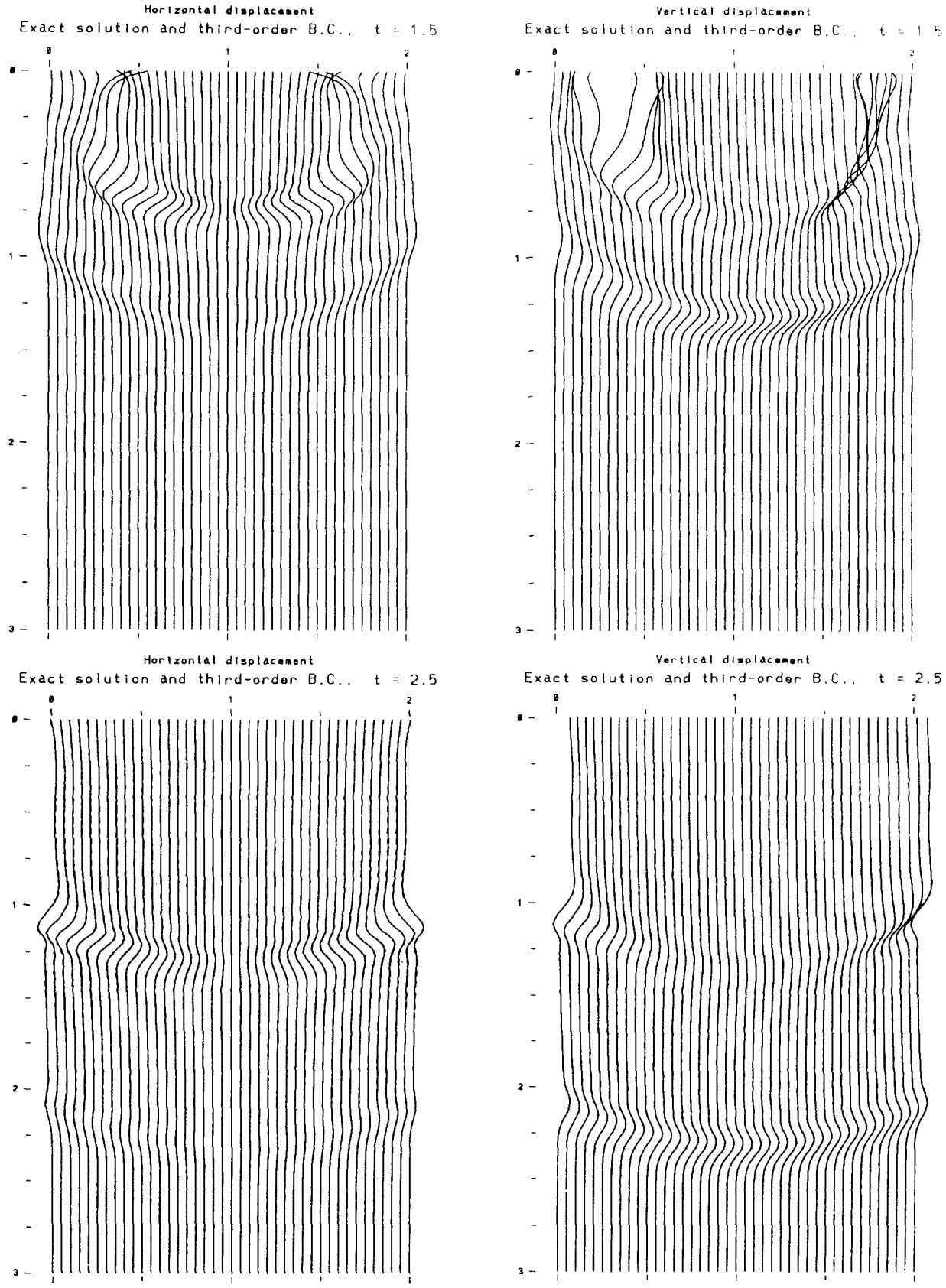

FIG. 5.3. Test 1. Solid curves show the exact solution. Dashed curves are used to plot the solution obtained with the third-order ($m = 3$) boundary condition, with $\beta_1 = 1$, $\beta_2 = c_P/c_S = \sqrt{3}$, and $\beta_3 = 1.3$. In most places, the dashed curves are not visible because the solutions agree to within the widths of the plotter lines.

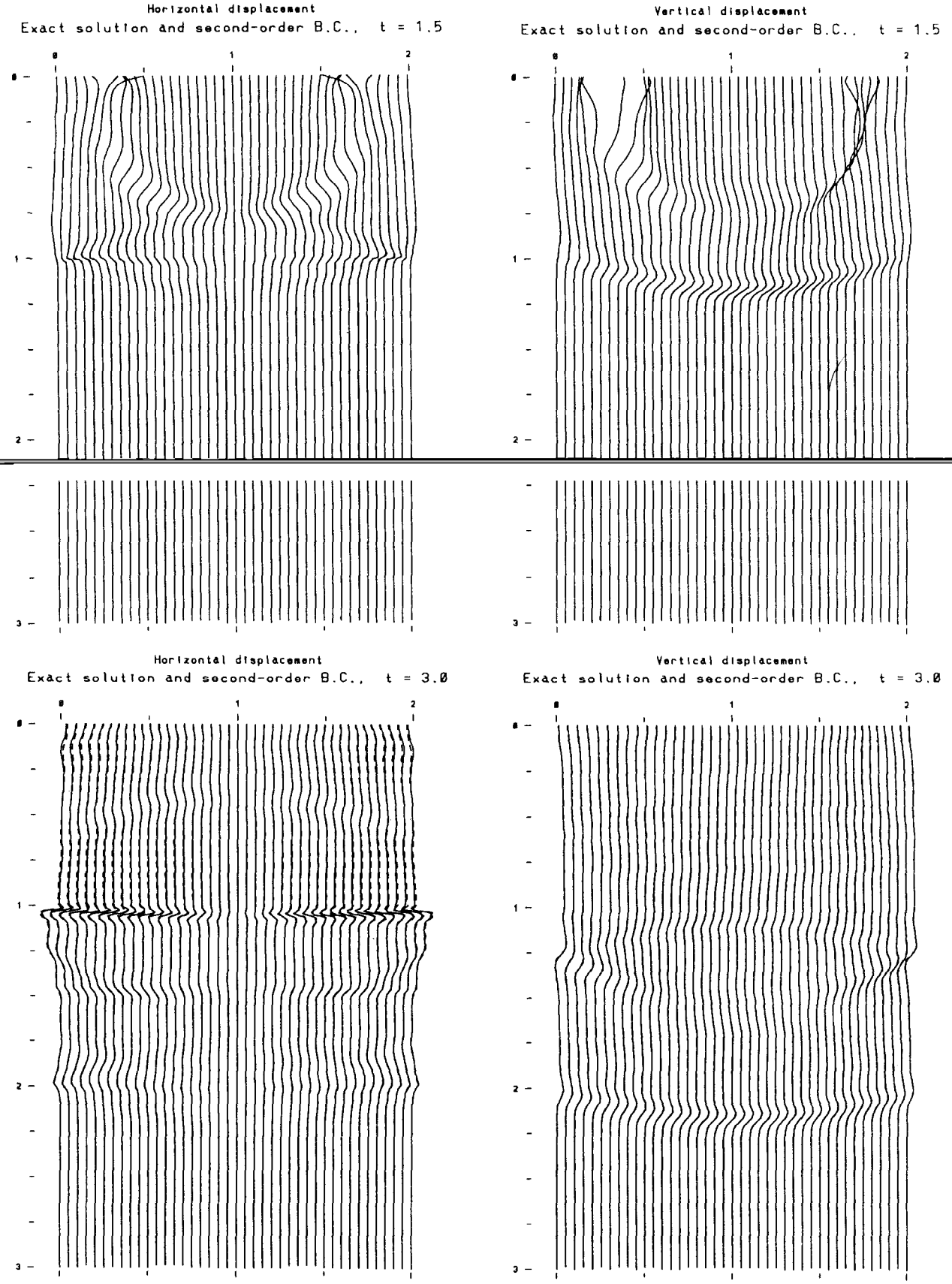

FIG. 5.4. Test 2. Layered medium. If $1 < z < 1.5$ or $2 < z < 2.5$, then the P-wave velocity is one-half the P-wave velocity elsewhere, and $c_S/c_P = 0.10$. In all other layers, $c_S/c_P = 1/\sqrt{3} = 0.577$. This is a severe combination of circumstances, due to the strong velocity contrasts between layers and the low value of c_S/c_P in two of the layers. The plots show the exact solution and the solution computed with the second-order boundary condition with $\beta_1 = 1$ and $\beta_2 = \sqrt{3}$.

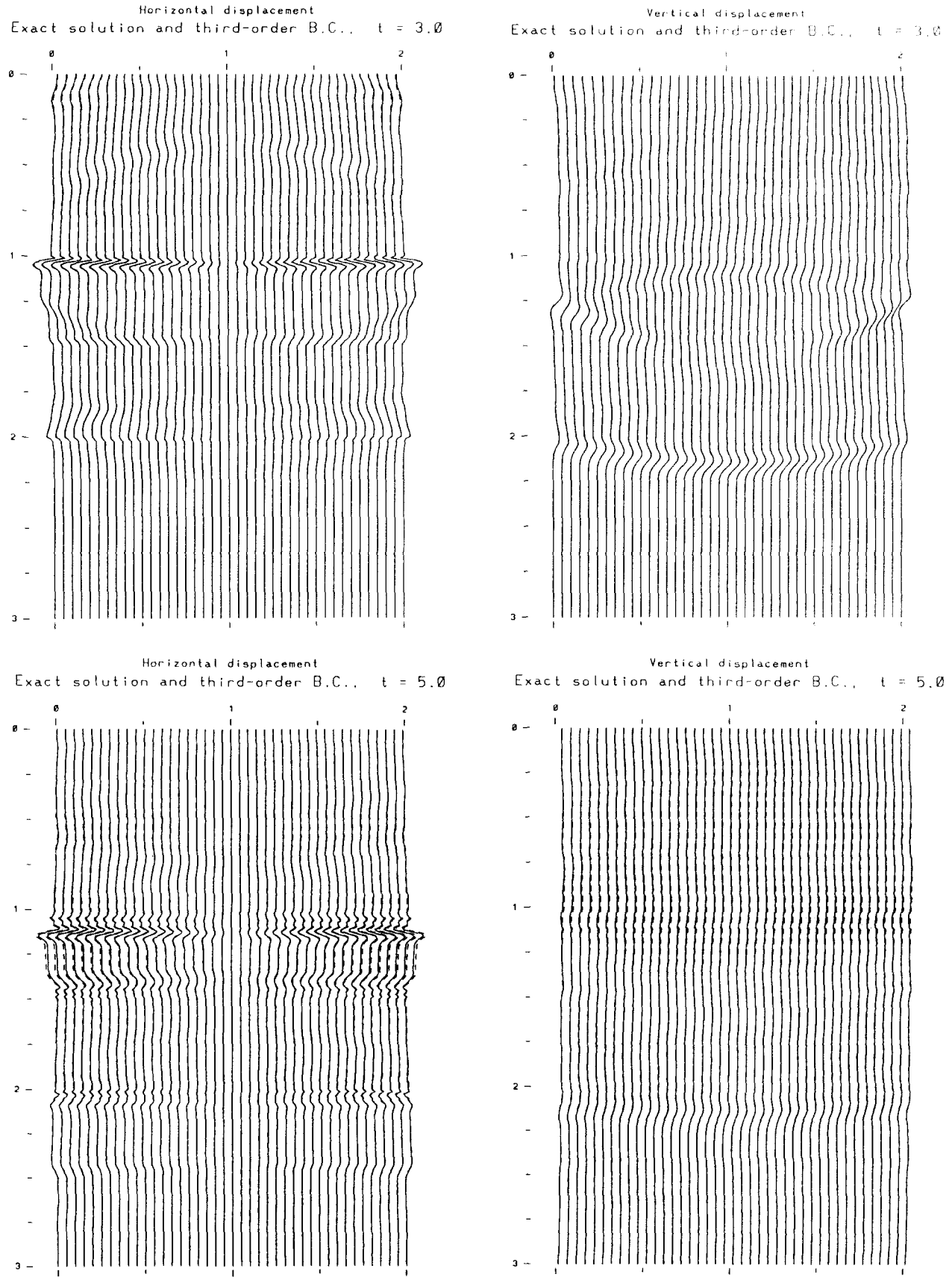

FIG. 5.5. Test 2. Long-time behavior, third-order boundary condition with $\beta_1 = 1$, $\beta_2 = \sqrt{3}$, and $\beta_3 = 3$. The solutions at time $t = 1.5$ are not shown because they are indistinguishable from the solutions at $t = 1.5$ shown in Fig. 5.4. By time $t = 5.0$, the primary reflections have long since returned to the surface, and the remaining activity consists mainly of slow S-waves in the second and fourth layers.

time step is $\Delta t = \frac{1}{100}$. The Courant number $c_P \Delta t/\Delta x$ is thus 0.8 in the fast layers and 0.4 in the slow layers. The source term (5.1) is centered at $x = 1$, its width in x is eight grid intervals, and its duration in time is 24 time steps. In the plots shown in Fig. 5.4, the displacements are amplified by a factor of 10 for the sake of visibility. The solution is plotted at every fourth grid point in x.

In Fig. 5.4, the solid curves show the exact solution at times $t = 1.5$ and $t = 3.0$. The dashed curves show the solution obtained with the second-order ($m = 2$) version of the boundary operator (3.7), with $\beta_1 = 1$ and $\beta_2 = \sqrt{3}$. At time $t = 1.5$, the L^2 reflection is 1.8% of the L^2 reflection produced by the homogeneous Dirichlet boundary condition. The reflection is 9.3% at time $t = 3.0$, 13.5% at time $t = 4.0$, and 23.1% at time $t = 5.0$. The third-order ($m = 3$) version of (3.7) was also used, with $\beta_1 = 1$, $\beta_2 = \sqrt{3}$, and $\beta_3 = 1.3$. In this case, the L^2 reflections are 0.3% when $t = 1.5$, 3.1% when $t = 3.0$, 5.6% when $t = 4.0$, and 11.0% when $t = 5.0$.

In these computations, the errows grow with time. This might not be of great significance, since by time $t = 5.0$ the primary reflections have long since returned to the surface,

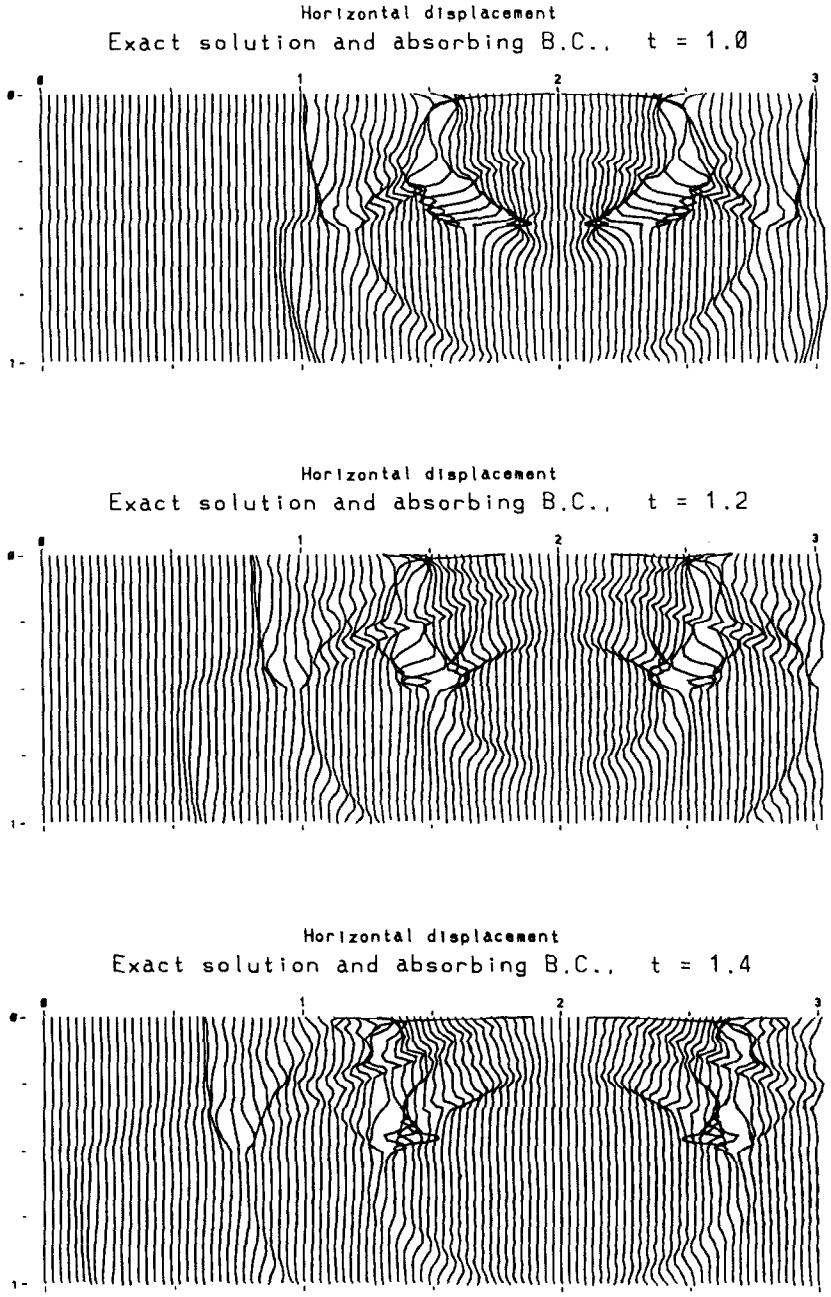

FIG. 5.6. Test 3. Layered medium. An interface is located at $z = 0.5$, and the P-wave velocity in the lower layer is twice the P-wave velocity in the upper layer. In each layer, $c_S/c_P = 1/\sqrt{3}$.

and the remaining activity consists mainly of slow S-waves in the second and fourth layers (see Fig. 5.5). However, the following remarks may be of interest.

Growth of error has been found regularly in two-dimensional computations. For example, see Figs. 7.1 and 7.2 of [10]; in those computations, growth of error was encountered with the boundary conditions developed in [10] and with the second-order boundary condition of Clayton and Engquist [3]. For the computations performed during the present tests, some plots of the solutions for $t = 5.0$ (not shown here) show that the main error is smooth and is located away from regions of significant wave activity. The effect is similar to, but more pronounced than, the error seen just above $z = 1$ in the plot of horizontal displacement at time $t = 3.0$ in Fig. 5.4. The smoothness and location of the error suggests that it may be related to the fact that Huyghens' principle does not hold in two dimensions; a sharp pulse is not propagated by a sharp signal, but instead the wave front is followed by a gradual decay. This effect is quite visible in the waves that are generated by the source used here. For example, see the vertical displacements near the free surface in Fig. 5.1 at $t = 2.5$ and in Fig. 5.4 at $t = 1.5$.

Because of these considerations, an additional experiment was performed with the third-order version of the boundary operator (3.7), with $\beta_1 = 1$, $\beta_2 = \sqrt{3}$, and $\beta_3 = 3$. The large value of β_3 corresponds to tuning the third factor in (3.7) to slowly moving waves; this choice is based on the idea of trying to absorbing slowly moving tails behind the main wave fronts. The L^2 reflections are 0.95% when $t = 1.5$, 4.0% when $t = 3.0$, 5.3% when $t = 4.0$, and 7.0% when $t = 5.0$. The results are better than those obtained with the second-order boundary condition. Also, with this choice of parameters in the third-order condition, there is better long-time behavior than with the choice mentioned earlier. The solutions at times $t = 3.0$ and $t = 5.0$ are plotted in Fig. 5.5.

Test 3. Layered medium, with waves moving downward into a faster layer. In this test, the computational domain is defined by $0 \leqslant x \leqslant 3$ and $0 \leqslant z \leqslant 1$. The medium consists of two layers, with $c_P = 1$ in the upper layer and $c_P = 2$ in the lower layer. The interface is located at $z = 0.5$. Within each layer, the velocity ratio is $c_S/c_P = 1/\sqrt{3}$. The densities are the same in the two layers.

The grid spacings are $\Delta x = \Delta z = \frac{1}{160}$, and the time step is $\Delta t = \frac{1}{400}$. The Courant number $c_P \Delta t/\Delta x$ is thus equal to 0.4 in the upper layer and 0.8 in the lower layer. The source term is centered at $x = 2$, and its durations in x and t are eight grid intervals and 24 time steps, respectively.

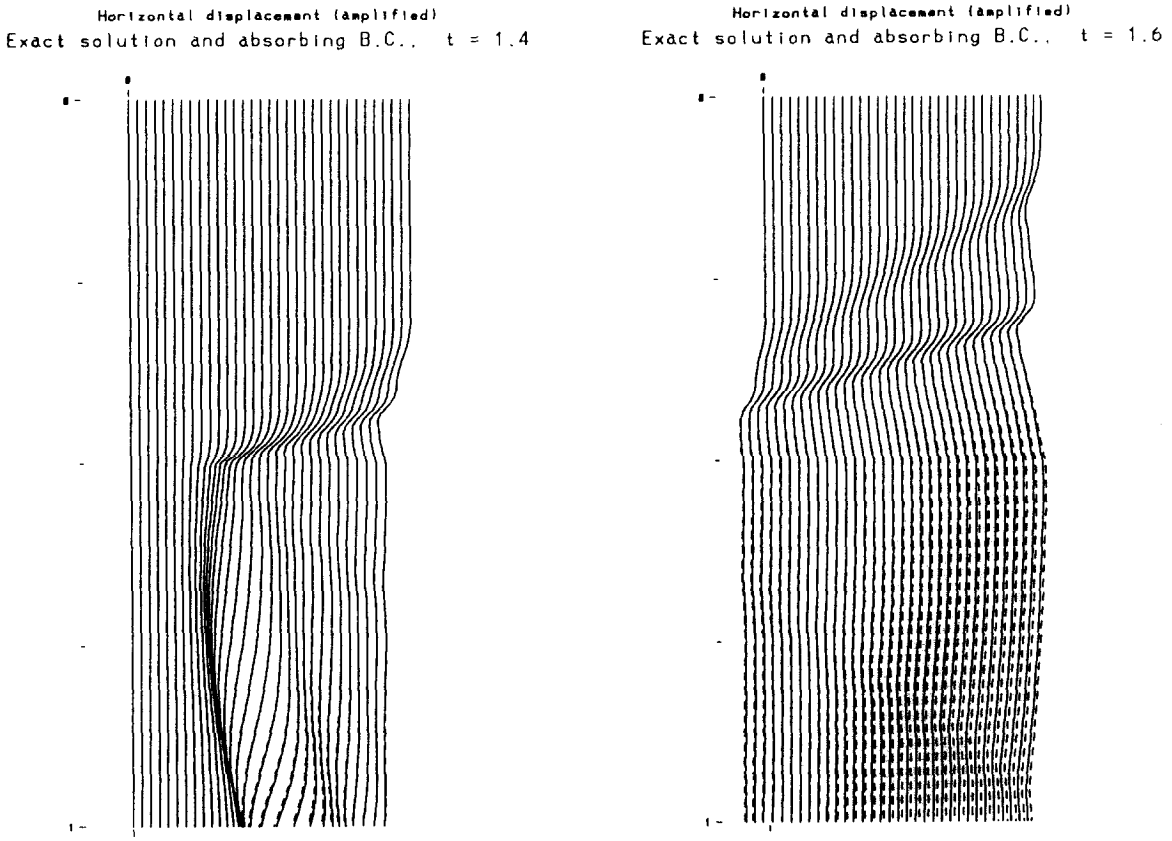

FIG. 5.7. Test 3. Close-up view of the left end of the computational domain. The solutions are plotted for $0 \leqslant x \leqslant 0.4$, and the displacements are amplified three times as much as in Fig. 5.6. The smooth error seen at time $t = 1.6$ is apparently related to Huyghens' principle; see the discussion of Test 2.

The horizontal displacements in the exact solution are shown by the solid curves in Fig. 5.6. By time $t = 1.0$, the downgoing P-wave generated by the source at the free surface has contacted the interface and has generated a transmitted P-wave and a transmitted S-wave into the lower layer. Upward reflections from the interface are also visible. The downgoing S-wave in the upper layer has also contacted the interface. The transmitted P-wave travels much more rapidly than all of the other waves in this system, due to the higher velocity in the lower layer, so it moves ahead of the other waves. At the point where this wave contacts the interface, the lower medium exerts forces on the upper medium and thereby generates waves that propagate into the upper medium. These waves, known as head waves, are visible in each of the plots in Fig. 5.6. There are two such waves; one is a P-wave, and the other is an S-wave.

In Fig. 5.6, the displacements are amplified by a factor of 100 instead of 10 in order to make the head waves more visible. The solution is plotted at every fifth grid point in x. The vertical displacements are not shown here because the main features of the solution are much more visible in the horizontal displacements. In particular, the particle displacements in the P-wave in the lower layer are nearly horizontal near the interface, so this part of the solution is not very visible in plots of vertical displacement.

In the computations that are shown here, the second-order ($m = 2$) version of the boundary operator (3.7) was used along the side boundaries, with parameters β_1 and β_2 chosen as follows. Along the interface, the head waves have the same apparent velocity as the P-wave that generates them. The boundary conditions used here are based on the apparent velocity, and we therefore chose β_1 so that it would give exact absorption of a normally incident P-wave in the lower layer. In the form (3.8) of the boundary operator for the lower layer, this would mean $\beta_1' = 1$. For the form (3.7), this is equivalent to $\beta_1 = 0.5$, since the P-wave velocity is twice as large in the lower layer as it is in the upper layer. The other parameter β_2 was chosen rather arbitrarily to be $\sqrt{3}$.

Along the bottom boundary, a third-order ($m = 3$) boundary condition was used. P-waves and S-waves near normal incidence are clearly an important issue in this case; so, in terms of (3.8), we used $\beta_1' = 1$ and $\beta_2' = \sqrt{3}$. However, when the P-wave in the lower layer approaches the lower left corner, its angle of incidence to the bottom boundary is not even remotely close to normal incidence. We made a

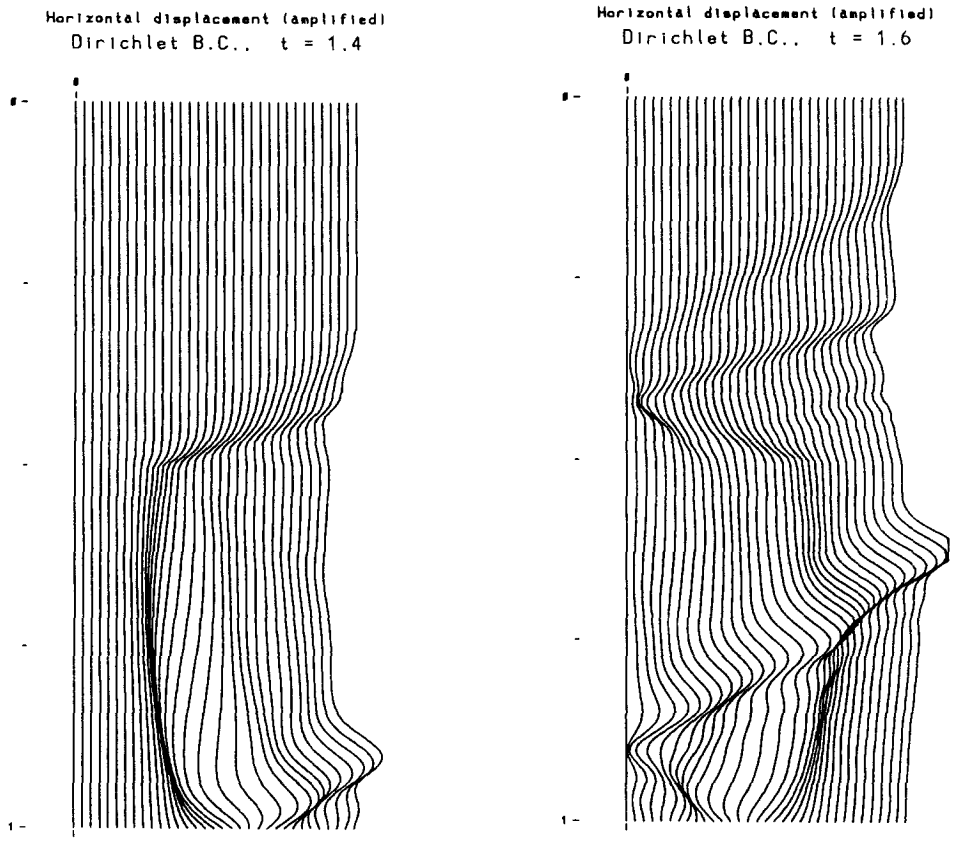

FIG. 5.8. Test 3. Solution using the Dirichlet boundary condition $u = w = 0$ along the side and bottom boundaries. Same plotting format as in Fig. 5.7.

rough guess of 70°, and then used $\beta_3' = \cos 70°$. For the equivalent boundary operator (3.7), the parameters are $\beta_1 = 0.5$, $\beta_2 = \sqrt{3}/2$, and $\beta_3 = (\cos 70°)/2$. In some additional tests, the third factor in the boundary operator was omitted. In this case, a slightly larger reflection was seen near the lower left corner; otherwise, the performance was very similar to the third-order case.

The solution computed with absorbing boundary conditions is plotted with dashed curves in Fig. 5.6. There is close agreement with the exact solution. The solution is symmetric about $x = 2$, and waves to the left of $x = 1$ are therefore mirror images of waves that have already encountered the computational boundary at $x = 3$. At time $t = 1.0$, the L^2 reflection is 1.2% of the L^2 reflection generated by the homogeneous Dirichlet boundary condition. The reflection is 3.1% when $t = 1.2$ and is 5.0% when $t = 1.4$. Figure 5.7 gives a close-up view of the P-wave in the lower layer and the head waves that it generates. For the sake of visibility, the displacements are amplified by a factor of 300 instead of 100. The solution is shown for $0 \leqslant x \leqslant 0.4$, and curves are plotted at every other grid point in x. For comparison, the solution using the Dirichlet boundary condition is shown in Fig. 5.8.

As in the previous test, effective absorption is obtained when the same boundary operator is used in each layer, even though the medium varies greatly from one layer to another.

I thank Kenneth Bube, Robert Keys, Alan Levander, and Børge Rosland for useful comments regarding the geophysical context of the matters discussed in this paper. This material is based upon work supported by the National Science Foundation under Grant No. DMS-8802649.

REFERENCES

1. K. Aki and P. G. Richards, *Quantitative Seismology: Theory and Methods*, Vols. I, II (Freeman, San Francisco, 1980).
2. K. E. Bullen and B. A. Bolt, *Introduction to the Theory of Seismology* (Cambridge Univ. Press, Cambridge, UK, 1985).
3. R. Clayton and B. Engquist, *Bull. Seismol. Soc. Am.* **67**, 1529 (1977).
4. S. H. Emerman and R. A. Stephen, *Bull. Seismol. Soc. Am.* **73**, 661 (1983).
5. B. Engquist and A. Majda, *Math. Comput.* **31**, 629 (1977).
6. B. Engquist and A. Majda, *Commun. Pure. Appl. Math.* **32**, 313 (1979).
7. D. Givoli and J. B. Keller, *Wave Motion* **12**, 261 (1990).
8. R. L. Higdon, *Math. Comput.* **47**, 437 (1986).
9. R. L. Higdon, *Math. Comput.* **49**, 65 (1987).
10. R. L. Higdon, *SIAM J. Numer. Anal.* **27**, 831 (1990).
11. R. L. Higdon, *Geophysics* **56**, 231 (1991).
12. J. B. Keller and D. Givoli, *J. Comput. Phys.* **82**, 172 (1989).
13. K. R. Kelly, R. W. Ward, S. Treitel, and R. M. Alford, *Geophysics* **41**, 2 (1976).
14. R. G. Keys, *Geophysics* **50**, 892 (1985).
15. H.-O. Kreiss, *Commun. Pure Appl. Math.* **23**, 277 (1970).
16. E. L. Lindman, *J. Comput. Phys.* **18**, 66 (1975).
17. K. D. Mahrer, *Geophysics* **51**, 1499 (1986).
18. C. J. Randall, *Geophysics* **53**, 611 (1988).
19. C. J. Randall, *Geophysics* **54**, 1141 (1989).
21. L. N. Trefethen and L. Halpern, *Math. Comput.* **47**, 421 (1986).
22. J. E. Vidale and R. W. Clayton, *Geophysics* **51**, 2247 (1986).